

# Lawrence Berkeley National Laboratory

## Chemical Sciences

### Title

Ambient pressure photoelectron spectroscopy: Practical considerations and experimental frontiers

### Permalink

<https://escholarship.org/uc/item/07q8f69p>

### Journal

Journal of Physics Condensed Matter, 29(5)

### ISSN

0953-8984

### Authors

Trotochaud, Lena  
Head, Ashley R  
Karslıoğlu, Osman  
[et al.](#)

### Publication Date

2017-02-08

### DOI

10.1088/1361-648x/29/5/053002

Peer reviewed

*Ambient Pressure Photoelectron Spectroscopy:  
Practical Considerations and Experimental Frontiers*

Lena Trotochaud,<sup>1†</sup> Ashley R. Head,<sup>1†</sup> Osman Karslıoğlu,<sup>1†</sup> Line Kyhl,<sup>1,2†</sup> and Hendrik Bluhm<sup>1\*</sup>

<sup>1</sup> Chemical Sciences Division, Lawrence Berkeley National Laboratory, Berkeley, CA 94720  
USA

<sup>2</sup> iNANO, University of Aarhus, DK-8000 Aarhus C, Denmark

\* Corresponding author: [hbluhm@lbl.gov](mailto:hbluhm@lbl.gov)

† These authors contributed equally

## Introduction

Processes at heterogeneous interfaces play a vital role in many areas of technology and in the environment. A fundamental understanding of interfaces under realistic conditions is a prerequisite for, e.g., the rational design of more efficient catalysts and electrochemical devices, as well as improved climate models through more precise input data on the fate of aerosols in the atmosphere, which is governed to a large degree by their surface chemistry. Over the last 50 years, the field of surface science has developed numerous techniques to prepare clean, well-ordered surfaces, including adsorbates, and to investigate them on the atomic scale with high elemental, chemical, and spatial resolution [1]. In general, these investigations require ultrahigh vacuum conditions in order to maintain control over the cleanness of the surface and the molecules adsorbed to it over the course of the experiment. Additionally, in the early days of surface science, a number of surface-sensitive spectroscopies required operation under vacuum conditions.

It was recognized early on that for the study of many important interface phenomena, investigations under elevated pressure conditions are essential to overcome the so-called “pressure gap”, which arises from the difference of the chemical potential of a gas at typical ultrahigh vacuum conditions ( $10^{-9}$  Torr) as compared to realistic pressures in a technical process or in the environment. For instance, realistic partial pressures of CO in hydrogen polymer electrolyte fuel cells are about 0.04 Torr (50 ppm) [2], and in Fischer-Tropsch reactions in excess of 10 bar [3], *i.e.* seven and twelve orders of magnitude higher than in ultrahigh vacuum, which corresponds to differences in the chemical potential 0.4 eV and 0.8 eV, respectively [4]. Other parameters that need to be controlled for measurements at realistic operating conditions (depending on the system under investigation) include e.g. temperature, applied potentials, and illumination. The measurement of interfacial processes at realistic conditions also requires the investigation of more complex, often multicomponent samples, as opposed to single crystal surfaces. Many catalysts today consist of metal nanoparticles supported on high-surface area oxides [5]; the high surface-to-bulk ratio in metal nanoparticles, their high number of under-coordinated surface sites, and metal-support interactions (including reactions at the interface between the metal and oxide) can all dramatically alter the reactivity of a metal nanoparticle compared to an extended, well-ordered, single crystalline surface. Industrial catalysts (or, to take an example from atmospheric chemistry, aerosol particles) are too complex to understand on a

fundamental basis using current experimental and theoretical methods. Carefully designed and prepared model systems capture some of the complexities of an industrial catalyst while being sufficiently well-defined to allow for an analytical understanding of the fundamental reaction processes. This approach is an important step toward realistic surface science studies, and great progress has been made in this area over the past decades [6,7].

Ambient pressure X-ray photoelectron spectroscopy (APXPS) is one among a number of surface-sensitive techniques that are being used to study surfaces and interfaces at elevated pressures, including vibrational sum frequency generation [8,9], scanning probe microscopy [10-13], electron microscopy [13,14], and X-ray absorption spectroscopy [15]. APXPS combines the advantages of vacuum-based XPS, namely chemical and elemental specificity, high surface sensitivity and quantitative analysis of the surface composition, with operation at elevated pressures. The principal obstacle to overcome in APXPS is the scattering of electrons by gas molecules; attenuation of the photoemission signal is a function of gas type, pressure, and the distance that the electrons travel in the presence of the gas. For instance, the inelastic mean free path of 100 eV kinetic energy electrons in 1 Torr of water vapor (i.e. close to the minimum of the mean free path [16]) is about 1 mm. All APXPS designs, therefore, aim at minimizing the path length of the electron trajectories in the high-pressure region. The first APXPS instruments were designed by the Siegbahn group in Uppsala in the early 1970s [17,18] and were followed by several other designs [19,20], all using laboratory X-ray sources (anodes). In the late 1990s the first synchrotron-based instruments were developed [21,22], resulting in an expansion of the APXPS user base. Subsequent commercialization of APXPS instruments [23,24] caused a rapid growth in the number of APXPS facilities, both synchrotron- [25] and laboratory-based.

The design of APXPS instruments has been described in a number of previous reviews [26-36] and will not be discussed in this article in detail. Briefly, most of the current APXPS instruments consist of a sample chamber that can be backfilled with a gas or gas mixture. Electrons (and gas molecules) enter the differentially-pumped electrostatic lens system of the APXPS spectrometer through a small aperture (< 1 mm diameter). The sample is brought close to the aperture to reduce the path length of the electrons through the gas. Several differentially-pumped electrostatic lens stages convey the electrons to the entrance of a hemispherical electron analyzer and maintain high-vacuum conditions around the electron detector at the exit of the hemispherical analyzer. Typical sample cell pressures in APXPS are in the Torr range, but under

special circumstances, APXPS can now also be performed at pressures up to 1 bar (see discussion below) [37]. The X-ray source itself must also be operated at UHV, and thus incident photons pass through an X-ray transparent window (typically  $\text{SiN}_x$  or thin aluminum) or a differential pumping stage that physically separates the gas environment from the UHV photon source (either lab-based anode or synchrotron beamline).

This review focuses on exemplary cases of APXPS experiments, giving special consideration to experimental techniques, challenges, and limitations specific to distinct condensed matter interfaces. We have organized this material into two different classes of interfaces: interfaces with vapor and buried interfaces. We begin with discussions of APXPS experiments on solid/vapor interfaces (including an extensive discussion of the special case of 2D films of graphene and hexagonal boron nitride on metal substrates with intercalated gas molecules) and liquid/vapor interfaces. We then discuss buried liquid/solid interfaces, which are a relatively new class of interfaces being probed by APXPS. Finally, we end this review with a critical evaluation of the persistent limitations and challenges of APXPS, as well as the current experimental frontiers.

## **Solid/Vapor Interfaces**

### ***General considerations***

Investigations of solid/vapor interfaces have been the workhorse of APXPS since its inception. It is easy to understand why this is the case, given the numerous relevant applications, in catalysis, corrosion, filtration, energy materials, and atmospheric science, [26,38-41] as well as the generally relative simplicity of the preparation and measurement of solid/vapor interfaces compared to, e.g., measurements of liquid interfaces. In particular, there has been great interest and success in recent years in applying APXPS to the study of “real” and “model” catalytic systems [31,42,43] and electrochemical devices [34,39,44]. For brevity’s sake, we will focus here on selected specific examples which highlight the strengths and limitations of the APXPS technique as it relates to the study these of solid/vapor interfaces.

Experiments on solid/vapor interfaces are performed using either a self-contained gas cell that is located within a UHV chamber or the entire experimental chamber is backfilled with gas to the desired pressure (see Figure 1). In addition, more complex gas cell designs have been used to study, for example, solid oxide fuel-cell systems, where the anode and cathode are separated by a conductive electrolyte membrane and each electrode is exposed to a different gaseous environment [45-47]. A common requirement in all of these schemes is that the distance from the sample surface to the differentially-pumped entrance aperture of the electrostatic lens system must be larger than two aperture diameter in order to avoid disturbances to the pressure distribution at the sample surface by the presence of the aperture [22]. (It was recently found that for certain configurations, the sample distance can be reduced to approximately one aperture diameter at pressures in the range of several Torr without significantly compromising the pressure at the sample surface [48].)

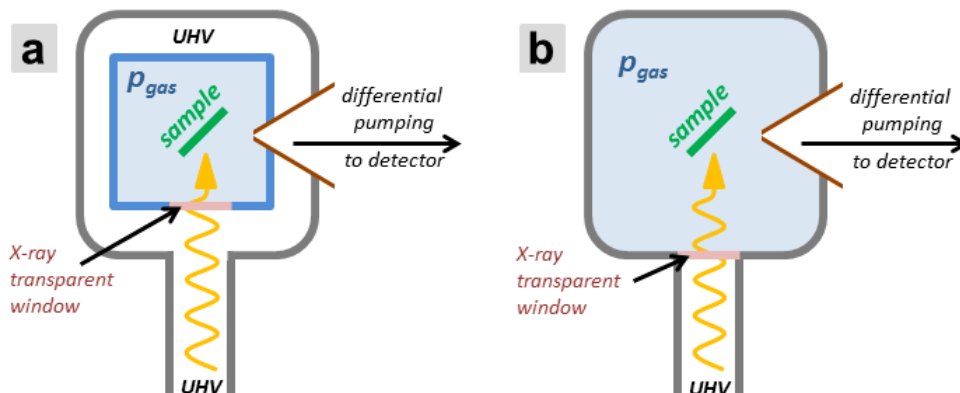


**Figure 1.** Introduction of the gas phase in APXPS studies of solid/vapor interfaces is typically accomplished by (a) use of a self-contained gas cell within the UHV chamber or (b) dosing the full chamber volume to the desired gas partial pressure  $p_{gas}$ . Figure not to scale.

The self-contained gas cell (Figure 1a) offers advantages that include the ability to quickly switch between several gases, option to flow gases across a sample instead of being in static equilibrium, return to UHV conditions after elevated pressure conditions, and ease of cell cleaning after experiments [35]. The second option (Figure 1b) is less complex and thus easier to use. Cross-contamination between different experiments is a major concern, particularly for synchrotron end stations, where multiple users conduct experiments in a relatively short time frame with numerous (possibly incompatible) gases with a wide variety of chemical reactivity and elemental compositions. Contamination by gases is not just a concern of gas compatibility (with each other or the experimental chamber components themselves), but also of gas persistence. Spectral characterization of the initial “clean” sample surface is a critically important data point, collection of which can be problematic when particularly persistent (or “sticky”) gas molecules are used. Avoiding contamination from persistent gases can also result in costly delays for subsequent instrument users if a lengthy bakeout or other method of chamber cleaning is required (or if the method of cleaning proves to be insufficient). The primary disadvantage of the self-contained gas cell is that it complicates the logistics of the XPS measurement – routines for e.g. sample alignment and preparation, docking and transfer of the gas cell, and plumbing of lines for gas introduction must all be carefully considered and reevaluated for each gas cell design. On the other hand, the use of certain gas cell designs enables application of APXPS to higher pressure regimes [37,49], as will be discussed in more detail below.

At sufficiently high partial pressure of a component of the gas phase ( $p_{\text{gas}}$ ), typically well above 0.01 Torr, photoelectron and Auger lines from the gas phase molecules will be visible in the XPS spectra. The ability to simultaneously collect spectra containing chemical information for the solid surface, surface adsorbates, and gas phase species in close proximity to the sample surface is arguably one of the unique strengths of APXPS. On the other hand, depending on the composition of the sample and the spectral regions of interest, gas phase peaks may overlap with those of the surface species. Typically for an individual core level, e.g. O 1s, and for small gas molecules, the gas phase peaks and solid surface peaks are well resolved due to final state effects [50], but core level and Auger peaks of other elements can interfere with the primary core levels of interest. There is some flexibility in using a synchrotron radiation source, in that the incident photon energy can in principle be selected to shift Auger features out of the way; however, as shown in an example below [51], spectral interferences are not always avoidable in this way. Accounting for the gas phase during data analysis is assisted by collecting the gas phase spectra at the same  $p_{\text{gas}}$  as spectra collected at the solid surface. One additional advantage of measuring the gas phase under the same conditions (photon energy, flux) as the surface measurements is that it often enables the determination of sensitivity factors (in the absence of artifacts in the apparent photoemission cross section of the gas phase constituents [52]), thus aiding in the quantitative analysis of the peak areas arising from adsorbates and the substrate. The study of gas molecules alone constitutes an entire well-established field of research in and of itself [53], but will not be addressed in this review.

For precise control of  $p_{\text{gas}}$  during APXPS measurements, the pressure is monitored by a variety of gauges, depending on the pressure range. For  $p_{\text{gas}}$  below  $\sim 1 \times 10^{-4}$  Torr, this can be accomplished by use of a conventional ion gauge. However, it is possible for gas molecules (e.g. hydrogen [54,55] and water) to crack over the hot metal filament of the ion gauge; in the case of water, this can result in more facile hydroxylation of solid sample surfaces than would otherwise occur without the ion gauge. Calibration of a high-precision leak valve vs.  $p_{\text{gas}}$  in the experimental chamber prior to introduction of the sample can be implemented to avoid this issue.

The same sorts of adventitious surface contamination as experienced in traditional UHV studies is also a concern in APXPS, even more so due to limited pumping during experiments at elevated pressures, and the fact that even gases with ppm purity will have contamination partial pressures in the  $10^{-6}$  Torr range when dosed at 1 Torr. While the adventitious or “environmental”



carbon signal has often been used for calibration of the binding energy scale [56,57], the presence of carbonaceous contamination at the surface can severely limit the study of surface reactions due to overlap with spectral features of the species of interest and blocking of active surface sites for gas molecule adsorption/reaction. (It is generally recommended to use a more robust internal standard for binding energy calibration, e.g. a core level of known oxidation state and binding energy or the Fermi edge for metals, as the chemical states and composition of adventitious carbon are by no means universal.) Additionally, carbonaceous and other contaminants (e.g., water) present on the inner walls of the APXPS chamber can be displaced by gas molecules at higher  $p_{\text{gas}}$ , so that even when a clean surface can be prepared at UHV conditions, surface contamination can be enhanced during the APXPS measurements.

Preparation of a clean solid surface for APXPS typically involves several steps, some of which may be performed *ex situ* or in a UHV environment. A number of endstations (e.g., APXPS-1 at beamline 11.0.2 at the Advanced Light Source in Berkeley, CA [38,58]) have both a sample preparation chamber and a connected, but isolatable, experimental/analysis chamber, with the ability to dose various gases at controlled pressures in either chamber. The preparation chamber is equipped with a suite of standard surface science tools, including sputtering source (for surface cleaning), electron-beam evaporator (for thin-film sample deposition), and a low energy electron diffraction (LEED) detector (for confirming cleanness of single crystal samples). The sample holder can also be equipped with a ceramic heating element, facilitating removal of adventitious carbon species and enabling sample annealing after metal deposition or surface sputtering. After cleaning/preparation of the sample surface and before dosing with gas, the dual-chamber end station allows for transfer of the sample from the preparation chamber to the XPS analysis chamber without exposure to atmosphere. The clean sample surface can then be characterized by XPS (under UHV conditions) prior to exposure to the gas phase of interest.

The addition of a heating element to the sample holder is also critical for APXPS measurements in systems where the relevant reaction conditions are at elevated temperatures. Alternatively, a NIR laser can be mounted on the chamber to heat the samples. This option may be preferred for operation at higher gas pressures when high temperatures are required (gas molecules can absorb and thus dissipate heat from the sample surface, requiring higher applied currents to reach the target temperature) or if hot metallic components of the heating element, which often have catalytic activity, can react with gas phase molecules (e.g. cracking of propane

on the Pt leads of a ceramic heater). A thermoelectric (Peltier) element can be used to control temperatures below room temperature and ensure that the sample is the coldest point in the chamber, as required for instance for measurements of samples at 100% relative humidity [58,59] (see example [60] discussed below).

### ***Limitations***

One continuing criticism of the technique, in particular for applications in heterogeneous catalysis, is the so-called “pressure gap” between technological applications and instrumental capabilities. Despite the ability to collect spectra while dosing gases above 5 Torr with the combination of differential pumping and electrostatic focusing lenses (at least one example has been reported with XPS measurements taken under 100 Torr of H<sub>2</sub> – a gas with a very small scattering cross-section [61]), the highest pressures attainable by APXPS are nevertheless often an order of magnitude or more below typical operating conditions for many chemical reactions of interest. This means that the chemical potential of the reactant gases during APXPS experiments may be much lower than in the “real” system, and the kinetic reaction barriers, mass transfer, and surface adsorption processes during APXPS may be quite different from those in the relevant technological application. Furthermore, the equilibrium or quasi-equilibrium conditions during APXPS measurements may be far from equilibrium state of the “real” system (or it may be difficult to determine whether equilibrium is established at all). A specific example [51] of the spectral manifestations of this pressure gap is discussed in more detail below.

The high photon flux of synchrotron radiation sources increases the likelihood that sample damage by the X-ray beam will be observed during APXPS studies performed at a synchrotron facility. Furthermore, the X-ray beam may cause ionization of or chemical reaction between gas molecules, which can change the chemistry of the gas phase itself as well as the solid/vapor interface. Control experiments demonstrating the manifestation or absence of beam-induced sample or gas damage are essential for accurate interpretation of APXPS data [62].

Homogeneous and inhomogeneous charging of the sample surface can manifest in XPS spectra as shifts in the peak positions and peak broadening, respectively [62]. Ionization of gas molecules by the incident photons can generate charges which partially compensate for the charging at the solid surface. In fact, some insulating samples which show clear spectral indications of surface charging under UHV conditions are more easily measured using APXPS

[29]. However, the issue of charging of insulating samples is a persistent limitation of APXPS that is not necessarily unique to solid/vapor interfaces, and will be addressed at a later point in this review.

### ***Exemplary Cases***

#### *Metal and Metal Oxide Surfaces under Humid Conditions*

We first examine work by Yamamoto and co-workers [60,63] highlighting the value of directly comparing UHV and APXPS measurements of the same solid surface. In this case, the vapor phase is water, and its interaction with three different single crystal surfaces is investigated. Not only is the interaction of water with metal (oxide) surfaces relevant for a variety of technological and environmental chemical processes, but this work clearly demonstrates the utility of *in situ* XPS measurements with relation to more general concepts of chemical equilibria and wetting phenomena at such surfaces.

The authors first compare the interaction of water with the (111) and (110) crystalline facets of metallic Cu; see Figure 2 for the relevant O 1s spectra taken at 1 Torr at room temperature, corresponding to a relative humidity of 5%. Figure 2a shows the O 1s spectrum of the (110) surface, with the gas phase water peak near 536 eV binding energy (BE), well-separated by 2-5 eV from the broader peaks of surface species. The wetting behavior of the Cu(111) and (110) surfaces is quite different, as shown in Figure 2b. Under the same conditions (295 K and  $p_{\text{H}_2\text{O}} = 1$  Torr; 5% relative humidity), no adsorption/dissociation of water is observed on the Cu(111) surface, while the Cu(110) is partially covered with a mixture of OH groups and adsorbed H<sub>2</sub>O. This experiment gives a direct observation of the difference in activation barriers for water dissociation over the pure metal surfaces, which is higher for Cu(111) than for Cu(110).

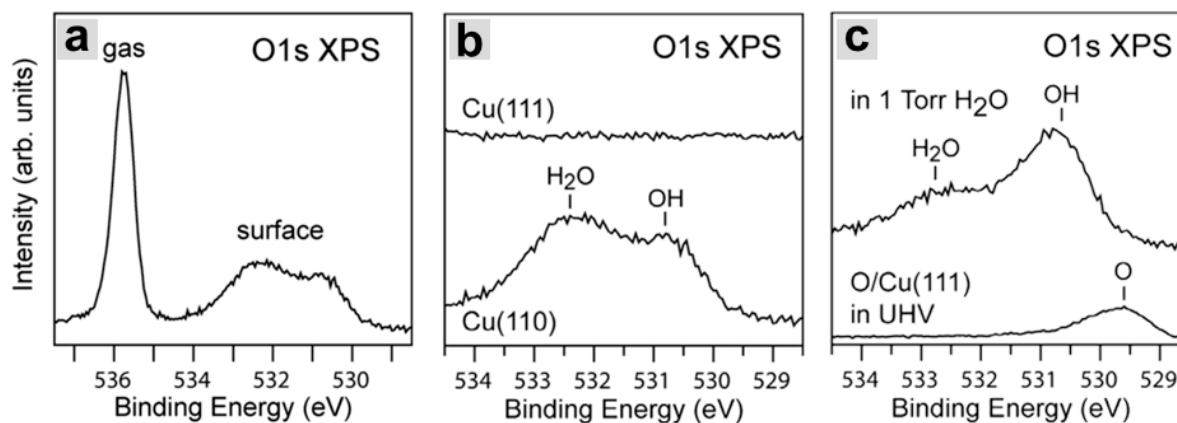


**Figure 2.** O 1s spectra of Cu(110) and Cu(111) surfaces at 295 K demonstrating the effects of different  $p_{\text{H}_2\text{O}}$  and surface pretreatments. Incident photon energy = 735 eV. (a) Cu(110) surface at  $p_{\text{H}_2\text{O}} = 1$  Torr (5% relative humidity at 295 K). The peaks for gas phase water and surface species are well-resolved, and the gas phase peak is not shown in subsequent spectra. © IOP Publishing. Reproduced with permission [63]. All rights reserved. DOI: 10.1021/jp0731654 (b) Comparison of Cu(111) and Cu(110) surfaces at  $p_{\text{H}_2\text{O}} = 1$  Torr. No O-containing surface species are observed on the Cu(111) surface, while Cu(110) spectra show partial coverages of 0.34 and 0.68 ML for OH and H<sub>2</sub>O, respectively. (c) Partially O-covered Cu(111) surface at UHV (lower) and  $p_{\text{H}_2\text{O}} = 1$  Torr (upper). Pre-adsorbed atomic oxygen on the Cu(111) surface reacts with water vapor, forming a mixed OH + H<sub>2</sub>O layer on the surface. (b) and (c) reprinted with permission from Yamamoto *et al.*, *J. Phys. Chem. B*, 2007, **111**, 7848-50 [60]. Copyright 2007 American Chemical Society.

Further analysis of the Cu(110) surface coverage as a function of temperature (not shown here) reveals two types of OH groups – those which form hydrogen bonds to water molecules and those which do not (OH<sub>pure</sub>). There is good agreement between the binding energies of OH<sub>pure</sub>, H<sub>2</sub>O, and mixed H<sub>2</sub>O+OH species measured in APXPS and those measured in previous studies at UHV conditions. One notable difference, however, between this work and previous UHV investigations is the absence of adsorbed atomic oxygen in the APXPS study. This absence is simply explained by the different reaction equilibrium conditions that exist under UHV vs. elevated pressure conditions for dissociation of water (see Equation 1). In UHV, formation of adsorbed atomic oxygen O<sub>ads</sub> and water by reaction of two surface OH<sub>pure</sub> sites is kinetically facile. In the presence of water vapor, the equilibrium is shifted in the opposite direction, favoring OH<sub>pure</sub> surface groups over atomic O<sub>ads</sub> [60,63].



**Equation 1.** Reaction equilibrium for dissociation of surface species on the Cu(110) surface. Increasing water vapor pressure  $p_{\text{H}_2\text{O}}$  shifts the equilibrium to the left (towards surface OH species), while lowering the system pressure (e.g. to UHV) drives the formation of adsorbed oxygen ( $\text{O}_{\text{ads}}$ ). The  $\text{OH}_{\text{pure}}$  nomenclature reflects surface hydroxyl species that are not H-bonded to water, as described in [60].

The importance of adsorbed atomic oxygen in the dissociation of water at metal surfaces is further illustrated by the spectra show in Figure 2c. Here, pre-treatment of the Cu(111) surface (exposure to  $1 \times 10^{-6}$  Torr  $\text{O}_2$  at 300 K, followed by annealing at 573 K [60]) leads to atomic O at the Cu(111) surface, which increases the hydrophilicity of the surface through a decrease of the dissociation barrier for water on O/Cu(111) compared to pure Cu(111) and generates a mixed  $\text{H}_2\text{O}+\text{OH}$  surface layer similar to that observed on Cu(110). This observation supports one of the main conclusions of this study: the formation of surface hydroxyls precedes adsorption of water [63].

We now turn attention to the dissociation of water on a metal oxide single crystal surface, namely  $\text{TiO}_2(110)$  [63,64]. These experiments highlight the importance of complementary UHV measurements of the clean sample surface prior to gas introduction. Initial UHV XPS measurements show that the clean  $\text{TiO}_2(110)$  surface always contains O-vacancy defects. Upon exposure to water vapor, the coverage of surface OH species is always twice that of the initial surface defect concentration. The O 1s spectrum of the clean surface is subtracted from spectra taken at higher water vapor pressures to calculate difference spectra (Figure 3) which more clearly show the evolution of surface water and hydroxyl species as a function of temperature (the O 1s spectra would otherwise be dominated by the signal from  $\text{TiO}_2$  lattice oxygen) [63].

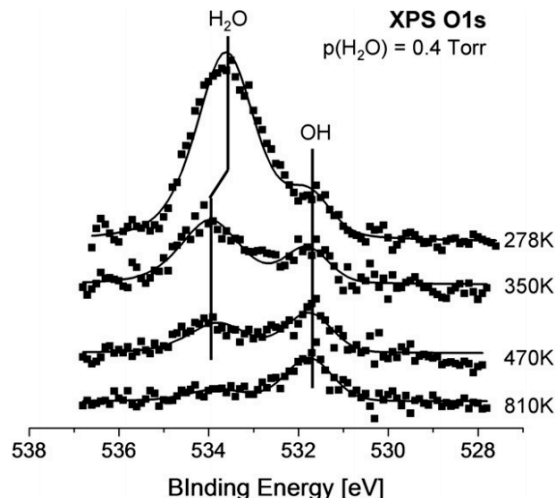


**Figure 3.** O 1s difference spectra of TiO<sub>2</sub> with  $p_{\text{H}_2\text{O}} = 0.4$  Torr at temperatures of 810 K, 470 K, 350 K, and 278 K (incident photon energy = 690 eV). Difference spectra were obtained by subtracting the spectrum measured in UHV before water exposure from each spectrum collected at a different sample temperature after normalization with the lattice oxygen peak. The gas phase water peak near 536 eV is removed by subtraction of the fitting line for the well-separated gas phase peak. Dots are the experimental data after the subtraction procedure and the thin solid line is the results from a least-square peak-fitting procedure. © IOP Publishing. Reproduced with permission [63]. All rights reserved. DOI: 10.1021/jp0731654

A combination of measurements collected at either the same temperature (isotherm) or  $p_{\text{H}_2\text{O}}$  (isobar) provide valuable insight into the process of water dissociation at the TiO<sub>2</sub>(110) surface. As mentioned previously, the coverage of OH on TiO<sub>2</sub> is determined by the surface defect concentration, and thus remains constant at all temperatures (Figure 4a) and water vapor pressures (Figure 4b). The coverage of water on the surface increases with increasing relative humidity until it is the same as that of OH (0.25 ML), after which the water coverage increases more rapidly. Note that Figure 4c shows the coverage data as a function of relative humidity (RH), recalculated from the measured isotherm (Figure 4b) and isobar (Figure 4a) data sets; since both data sets overlap when plotted against relative humidity, it can be concluded that kinetic barriers in these experiments are negligible. The data in Figure 4 were taken using two different sample holders, either equipped with a resistive heater or a Peltier cooler to measure the full relative humidity range. The Peltier cooler is used to measure at high relative humidity close to saturation, where a traditional cold finger cooling scheme would lead to condensation of water at the cooling lines and not the sample. In all data sets the OH coverage remains constant at 0.25

ML (twice the initial defect coverage) over the entire RH range, while the H<sub>2</sub>O coverage increases, with the rate of water absorption sharply increasing above ~90% RH [60,63].

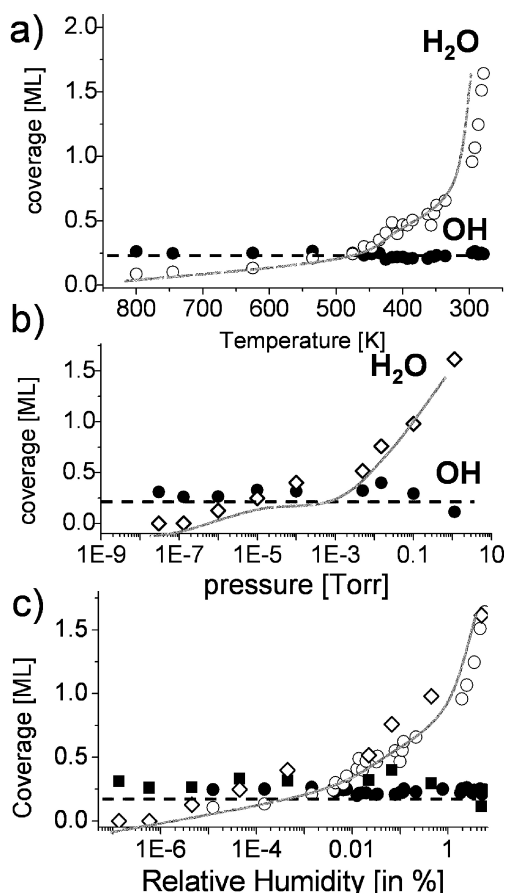


**Figure 4.** (a) Isobar ( $p_{\text{H}_2\text{O}} = 0.4$  Torr) and (b) isotherm ( $T = 298$  K) showing the water and OH coverage as a function of decreasing temperature and increasing pressure, respectively. (c) Same data plotted as a function of relative humidity. Empty diamonds and filled squares: isotherm; filled and empty circles: isobar. Both results collapse into the same curve, demonstrating that the surface and gas phase are in thermodynamic equilibrium. Dashed and solid lines are inserted as a visual aid. Reprinted with permission from Ketteler *et al.*, *J. Phys. Chem. C*, 2007, **111**, 8278-82 [64]. Copyright 2007 American Chemical Society.

As mentioned before, the “pressure gap” is the term used to describe the lingering discrepancy between the pressures available to APXPS and the pressures of many relevant technological applications. A recent work by Blomberg *et al.* [51] on a model catalyst system serves as an exemplary case study in what we can learn when we approach this gap and as a reminder that we still have many obstacles to overcome to bridge it successfully.

Figure 5 shows an intensity plot of the O 1s/Pd 3p region as a function of temperature during CO oxidation over Pd(100) in a 1:1 mix of CO and O<sub>2</sub> at a total pressure of 0.5 Torr. The darker black and red regions indicate low counts (near the background level), while the brighter red and yellow areas indicate higher peak intensities, respectively. The continuous series of spectra, collected during a heating ramp followed by a cooling period, show several features: (1) at ~345 °C, the gas and surface species suddenly change from adsorbed CO with CO and O<sub>2</sub> in the gas phase below ~345 °C, to adsorbed O with CO<sub>2</sub> and O<sub>2</sub> in the gas phase above ~345 °C; (2) heating further above this critical “activation temperature” does not significantly change the spectra; (3) the surface returns to its initial state upon cooling below ~225 °C. We can also see here an example where the core levels of two surface species (O1s of adsorbed CO and Pd 3p) overlap, but the line shapes are sufficiently different so that the two species can be de-convoluted during peak fitting (not shown here).



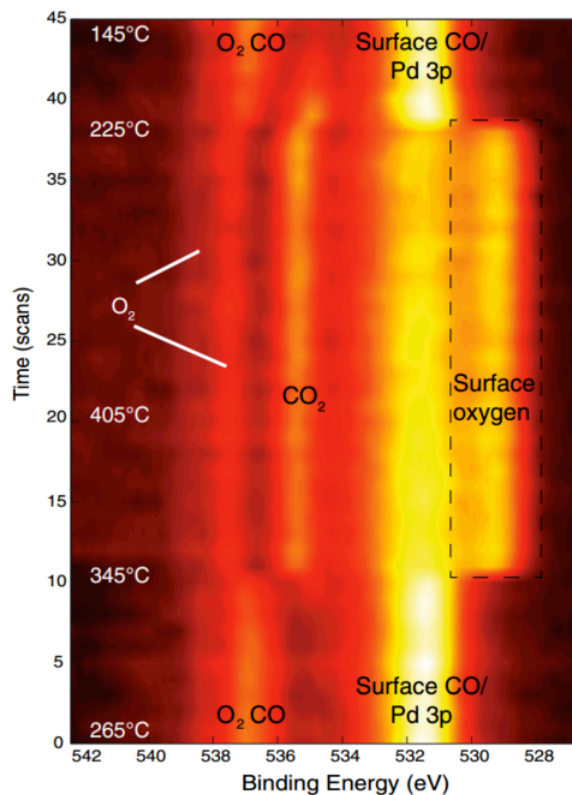


**Figure 5.** O 1s region during CO oxidation in a gas mixture of 0.25 Torr CO and 0.25 Torr O<sub>2</sub>. The temperature of the Pd(100) (shown to the left in the figure) was ramped up and down during the measurement. Reprinted figure with permission from Blomberg *et al.*, *Phys. Rev. Lett.*, 2013, **110**, 117601 [51]. Copyright 2013 by the American Physical Society. <http://dx.doi.org/10.1103/PhysRevLett.110.117601>

Above 345 °C, the surface catalytic activity is sufficiently high to convert all CO molecules at the surface into CO<sub>2</sub>; in addition, only gas phase CO<sub>2</sub> (i.e. the product) is observed near the sample surface. This result is a clear indication that under these experimental conditions, the reaction is mass-transfer limited and could imply that the Pd(100) surface with chemisorbed O is the active catalytic phase *under these conditions*. As the authors lay out in their introduction, however, the oxidation of Pd(100) under oxygen atmospheres is known to lead to surface or bulk oxidation of the Pd depending on the O<sub>2</sub> pressure (particularly at higher pressures approaching those that are technologically relevant for CO oxidation), and that the effect of CO on this oxidation process is still unclear. In these 1:1 CO:O<sub>2</sub> experiments, no evidence of Pd oxidation is found in either O 1s nor Pd 3d spectra.

Experiments performed at higher total pressures (up to 1 Torr) at 1:1 CO:O<sub>2</sub> or at higher O<sub>2</sub> partial pressures (1:4 CO:O<sub>2</sub>) do show evidence of Pd oxidation (Figure 6). Nevertheless, the

system still suffers from mass transfer limitations under these conditions, and a higher O<sub>2</sub> partial pressure results in a lower activation temperature. Extrapolation of these results to the likely termination at technological conditions suggests that a surface oxide dominates – a condition which is not captured here in the 1:1 stoichiometric experiments. In fact, the behavior of the solid surface in this work seems to change just at the threshold of pressures accessible to XPS, serving as a poignant reminder that the pressure gap is significant and should be approached with caution.

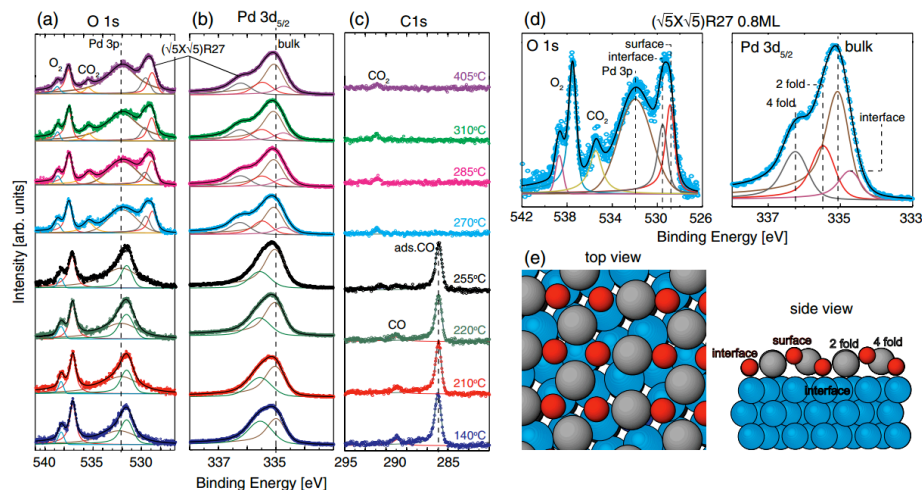


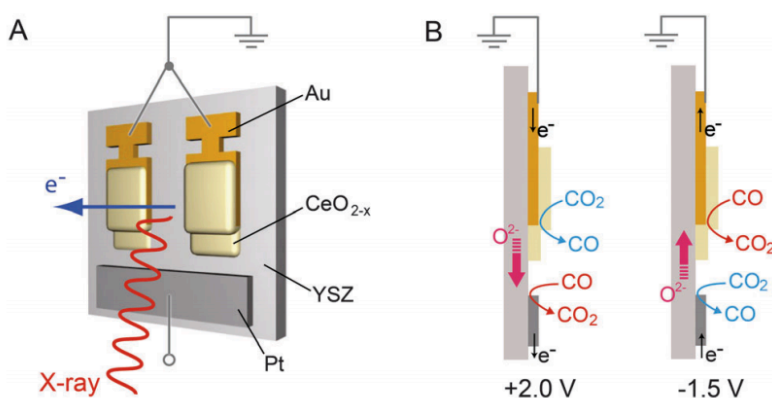
**Figure 6.** CO oxidation at 0.5 Torr and a 1:4 CO:O<sub>2</sub> partial pressure ratio. Shown are the binding energy regions of (1) O 1s, (b) Pd 3d, and (c) C 1s. (d) A more detailed view of the O 1s and Pd 3d spectra directly above activation temperature. (e) Structural model of the  $(\sqrt{5} \times \sqrt{5})$  surface oxide on Pd(100) according to [65,66]. Reprinted figure with permission from Blomberg *et al.*, *Phys. Rev. Lett.*, 2013, **110**, 117601 [51]. Copyright 2013 by the American Physical Society. <http://dx.doi.org/10.1103/PhysRevLett.110.117601>

The recent development of APXPS gas cells equipped with gas-impermeable single-layer graphene membranes [37] enables measurements at even higher pressures than those reported here, and exploration of the Pd/CO system with such a cell configuration could enable a direct measurement of the catalytically active species at more technologically-relevant gas pressures. However, there is the logistical requirement in this configuration that the graphene membrane acts as the catalyst support, which limits the sample to particles that can be deposited directly on the membrane and also introduces the possibility that the chemistry will be affected by catalyst/support interactions. While particles or polycrystalline samples may be closer to “real” catalyst systems, it is not currently possible to measure unsupported or single-crystal surfaces using such a configuration.

## Spatial Resolution in Electrochemical Devices

Spectroscopic characterization of chemical and electronic states across multiple length scales remains a grand challenge for the surface scientist. Electrochemical systems, such as solid oxide electrochemical cells (SOECs), are a particularly interesting class of materials in this regard, as changes in both chemical and electronic states across short length scales can determine the material properties of interest. We next examine two studies demonstrating the utility of APXPS for *operando* probing of changes in both chemical and electronic states in such systems.

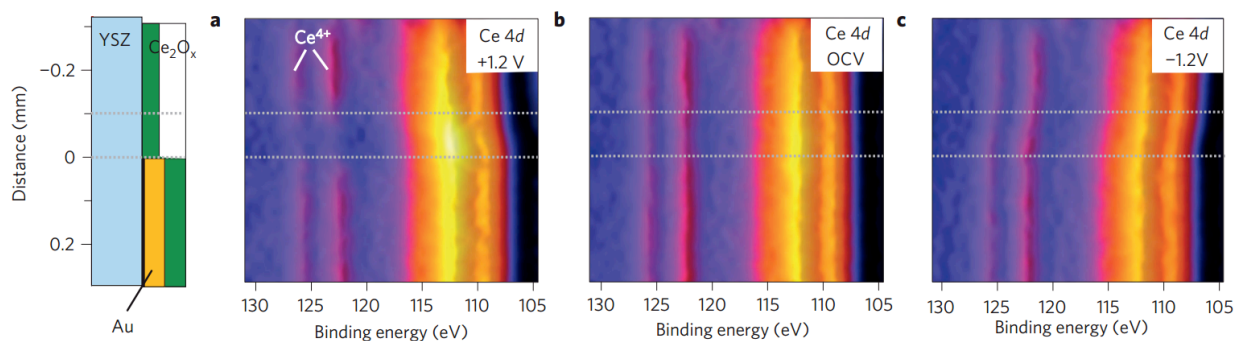
The thin-film SOEC design used in these works is shown schematically in Figure 7. The design of the SOEC is such that the Au/ceria working electrodes and Pt counter electrodes are deposited as thin films on the same side of the yttria-stabilized zirconia (YSZ) solid electrolyte. In this way, all cell components are simultaneously exposed to the gas phase and are easily accessible for APXPS measurements.



**Figure 7.** (A) Schematic illustration of the electrochemical cell comprising a 300 nm Pt counter electrode, a 300 nm Au current collector on top of a 50 nm alumina film (not shown) and a 350 or 1000 nm ceria working electrode patterned onto a polycrystalline YSZ substrate. (B) Schematic illustration of electro-chemical reactions under positive and negative biases. Reproduced from reference [67] with permission of the PCCP Owner Societies. <http://dx.doi.org/10.1039/C4CP01054J>

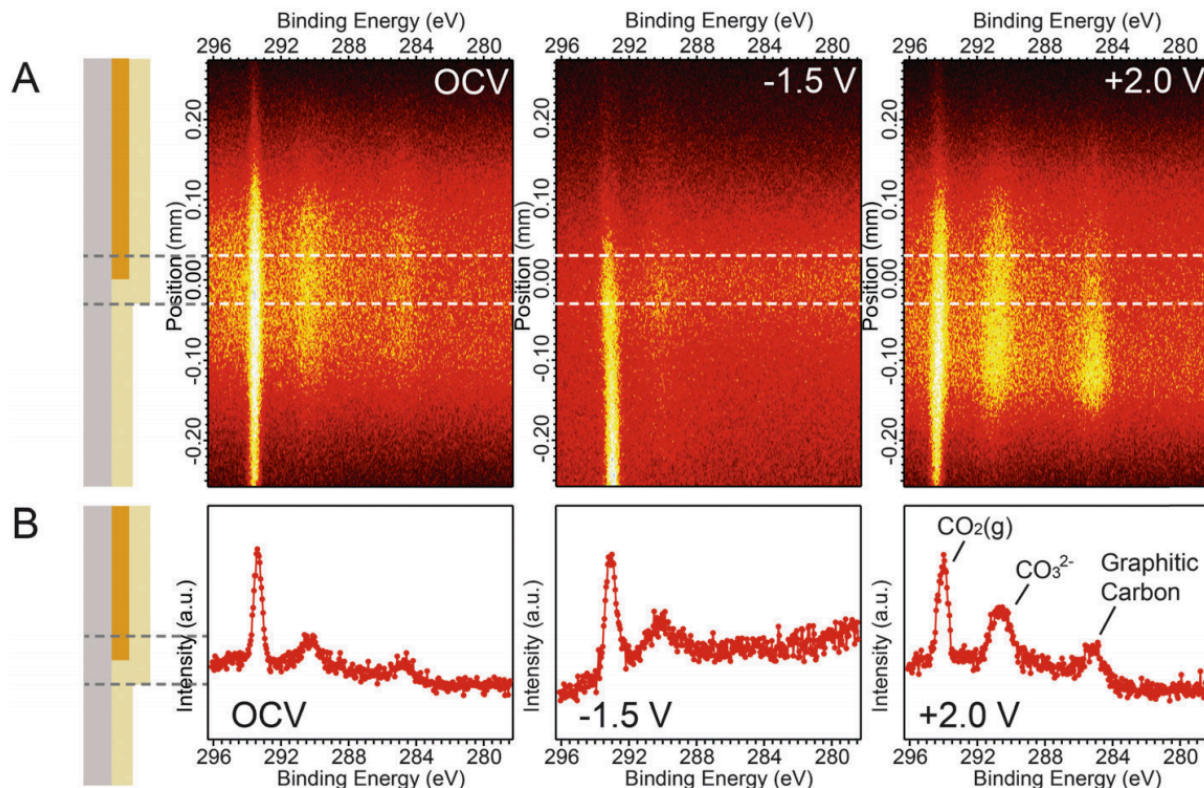
The distinct advantage of APXPS in studying electrochemical systems is the facile, contactless measurement of local potentials (even at elevated temperatures) across the different solid/solid interfaces in the SOEC – the working electrode is grounded to the APXPS analyzer, and thus the core level photoelectrons measured by APXPS show a shift in kinetic energy ( $\Delta KE$ ) that is related to the local potential ( $V_L$ ) by  $\Delta KE = eV_L$ . An example of this shift is shown in

Figure 8, where the apparent binding energy of the Ce 4d signal shifts in the electrochemically active spatial region as the applied bias is changed [68].



**Figure 8.** Distance-resolved XPS spectra of the Ce 4d region at +1.2, 0 and -1.2 V applied potential recorded with 490 eV photon energy (OCV = open circuit voltage). The dotted lines denote the electrochemically active regions corresponding to the schematic cell drawing on the left side. The ceria is 50 nm thick on the working electrode. Reprinted by permission from Macmillan Publishers Ltd: Nature Materials, copyright 2010 [68].

Use of a 2D area detector during APXPS data acquisition allows for a snapshot of the distribution of local chemical states across the different component interfaces in the SOEC devices [68]. In the case of ceria, changes in the ratio of  $\text{Ce}^{3+}/\text{Ce}^{4+}$  across the YSZ/ceria interface can be observed and quantified – the spatial region (in this case  $\sim 150 \mu\text{m}$ ) over which the Ce oxidation states vary from their equilibrium ratio is indicative of the electrochemically active region. This is confirmed by simultaneous electrochemical current measurements, as well as the core-level binding energy shifts observed in APXPS measurements. Furthermore, chemical intermediates of the solid/vapor surface reactions can be identified and when correlated to the applied bias and local potential of the electrodes, important information about kinetic limitations of the surface reactions can be deduced. Figure 9 shows C 1s spectra collected at a ceria surface in the presence of  $\text{CO}_2$  and with changes in the applied bias. Surface carbonate species at both oxidizing and reducing potentials indicates that this is an important surface intermediate in both electrochemical half-reactions. Additionally, differences in the steady-state concentrations of surface species at various applied biases is used to elucidate kinetic information about the electrochemical redox processes [67].



**Figure 9.** (A) Spatially-resolved XPS measurements of the C 1s obtained with a two-dimensional area detector at 0, -1.5 and +2.0 V applied potentials with 490 eV photon energy (OCV = open circuit voltage). A corresponding schematic cell drawing is given on the left. Color scheme is given in Figure 7. The ceria is 1000 nm thick on the working electrode. (B) Integrated spectra obtained by slicing a 60  $\mu\text{m}$ -wide segment from the corresponding photoelectron signal in (A) at position of 0.0 mm. Intensities are normalized to the CO<sub>2</sub> gas phase peak. Reproduced from reference [67] with permission of the PCCP Owner Societies. <http://dx.doi.org/10.1039/C4CP01054J>

These types of measurements are ultimately limited by the spatial resolution ( $\sim 10 \mu\text{m}$ ) of the detector. Improvements in detector hardware, as well as the option to employ scanning (as in scanning photoemission microscopy, SPEM [69]) or full field imaging (as in photoemission electron microscopy, PEEM [70]), are required to improve the spatial resolution, which is important for deconvolution and identification of surface species at discrete interfaces and across potential gradients in electrochemical systems. However, at the time of publication of this review, there is no ambient-pressure version of SPEM or PEEM available.

The above examples show the utility of APXPS to investigate important phenomena in environmental science, catalysis, and electrochemistry with high surface and chemical as well as

potential sensitivity. For the study of environmental processes, which are often governed by the presence of water vapor, one can postulate that the pressure gap has been essentially been bridged since investigations at up to 100% RH at room temperature (equivalent to ~20 Torr water vapor partial pressure) are now routinely possible; the partial pressure of other important trace gases in the environment is much lower (CO<sub>2</sub> with ~0.4 Torr being the highest). Pressure gap considerations are much more prevalent still in the case of catalytic reactions, where off-line reactor measurements under technologically relevant conditions (> 1 bar) and under the low pressure regime used in APXPS need to be performed. If critical reaction parameters, such as yield, selectivity, and conversion are similar in the low and high pressure regime, this would be a necessary but not sufficient condition for the relevance of APXPS experimental findings for technological applications.

In the next section, we will consider current investigations on a unique class of interfaces with a vapor phase, namely that between a (in most cases) monolayer solid film and bulk solid substrate with gas molecules intercalated between the solid layers, which has garnered a lot of attention over the past years due to the opportunities for tuning the chemical properties of the essentially two-dimensional space of the interface.

## **Solid/2D layer interfaces**

### ***General Considerations***

This section presents an overview of the advantages, limitations, and challenges of using APXPS for studying the interface of a solid surface and a two-dimensional (2D) layer. Research and development of novel 2D systems [71] such as hexagonal boron-nitride [72] (hBN), transition metal dichalcogenides (TMDC's) [73,74], phosphorene [41], and silicene [75] has expanded rapidly since the isolation and characterization of graphene in 2004 [76]. The members of the zoo of currently available 2D materials offer different electronic [74,76-78], optical [74,77,79], and chemical properties [80]. A typical 2D layer is either “grown” directly on a transition metal substrate or exfoliated from its bulk counterpart (for graphene this is graphite) and transferred to a substrate of interest. In some cases, a chemical transformation such as reduction of graphene-oxide to graphene [81,82] or reduction of MoO<sub>3</sub> to MoS<sub>2</sub> [83] is a viable route to obtain the 2D material of interest. The growth of 2D materials on transition metal substrates by chemical vapor deposition (CVD) method typically requires exposing the hot metal surface to relevant chemical precursors [84-86]. Usually the pressure of the gaseous precursors is too high for studying the growth by *in situ* methods and knowledge about the growth mechanisms have been based on accumulated partial growth followed by characterization at each step [87] and/or by comparing the results obtained by a simple variation of the growth parameters [88,89]. APXPS, however offers new possibilities to gain insight into the growth mechanisms as shall be exemplified in this section.

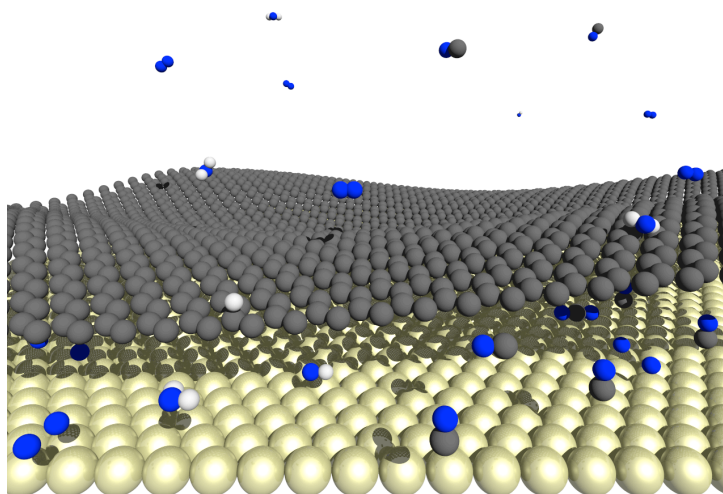


**Figure 10.** Schematic of a metal/2D layer interface, exposed to various gases, exemplified by graphene on an Ir(111) surface.

The choice of substrate as well as the method of preparation has a pronounced influence on the properties of the layer. This includes the electronic or structural properties in the form of changed curvature or induced lattice strain in the 2D layer, as has been shown for graphene [90]. This may affect the reactivity and permeability of the otherwise inert and impervious structure, which can be studied by APXPS measurements. Besides considering the choice of substrate, the properties of an interface may be altered by intercalation. Intercalation refers to introducing molecular or atomic species in the 2D layer-substrate interface (e.g. as depicted in Figure 10). The intercalation procedure has been widely studied for graphene on a range of metal substrates using different gases and metals with the aim of weakening the intrinsic metal-graphene interaction and a subsequent recovery of freestanding graphene properties [91-94]. An acknowledged conclusion for the mechanism of intercalation of graphene-substrate interfaces is that it proceeds through atomic- or structural defects, domain or sheet boundaries, wrinkles or other areas of strained graphene [94-97] and thus not through the intrinsic, defect free basal plane which is considered impermeable for all species except protons [98]. The details of the intercalation mechanism depend on the system, i.e. the substrate, 2D layer (type, quality, rotation, etc.), and intercalating species. For many systems, high pressures and/or elevated temperatures are required for the intercalation to occur, making APXPS ideal and in many cases necessary for such studies. The limited sensitivity of APXPS to the presence of defects, however, makes it



difficult to determine the exact mechanism solely using this technique (see below for further discussion).

More recently the intercalation at hexagonal boron nitride (h-BN)/metal [99,100] and SiO<sub>2</sub>/metal [101] interfaces have also been observed. In this section, we will focus on graphene and h-BN and intercalation.

### ***Limitations***

New approaches and challenges arise for studying 2D-layer interfaces under ambient pressures. For both growth and intercalation purposes, the sample surface has to have a high level of cleanness. For example, it was shown that the gap at the graphene edges on Pt(100) may be sealed by oxygen atoms binding between C atoms on the edge and Pt atoms on the surface [102]. In the presence of hydrogen, however, hydroxyl groups could form and bind to the graphene edge, resulting in an opening of the edge facilitating intercalation of gaseous species. Surface contamination may thus alter the outcome of an intercalation experiment and caution towards chamber cleanliness must be taken. It may additionally be impossible to detect such unpredicted edge or defect functionalization on a 2D layer using (AP)XPS due to their low population. This issue of sample cleanness becomes increasingly important and more difficult at high pressures, requiring high purity gases in addition to a clean sample surface and measurement chamber.

Questionable reproducibility of preparing samples of a certain quality in various experiments and systems yields another challenge for comparing results. Caution must be taken towards proper characterization of the 2D layer. For example, a sample characterized by XPS and deemed of high quality may exhibit atomic scale defects visible in STM. Standard low electron energy diffraction (LEED) is a popular method of 2D layer sample characterization, where the presence of *some* ordered domains of a single rotation yields a well-defined LEED pattern, but usually leaves out any information of the presence of non-crystalline amorphous areas on the surface. It is, thus, challenging to study a system using a single characterization method only, and even though APXPS can provide unique *in situ* information, it should optimally be combined with other methods.

Additionally, the presence of atomic or structural defects has a high influence on the reactivity, and the study of defects in a more realistic, non-ideal 2D layer provides a whole

segment of research by itself. What should be mentioned here is that the defect density can be very low while still having a high influence on the material properties. Studying the effect of such defects of low density by APXPS induces a challenge of sensitivity, which typically requires a few percent of a monolayer (ML) for detection of surface species. An interesting relevant example is the reported “metal-free” catalytic activity of graphene and carbon-based materials for e.g. the oxygen reduction reaction (ORR) [103-109], which has recently been proposed to actually stem from trace amounts of reactive metal particles (residues from synthesis procedures) and not the carbon material itself [110]. The quantity of these residues is, however, too small to be detected by most characterization methods, including (AP)XPS, and their presence is proposed to be detected by ICP-MS/OES, X-ray fluorescence, or neutron activation analysis [110]. For the detection of very low concentration defects and adatoms on 2D layer systems, we also suggest HREELS [111,112] with a sensitivity as good as  $10^{-3}$  ML [113] as a complementary technique to APXPS.

### ***Exemplary Cases***

#### *2D-Layer Growth Mechanism*

The growth mechanisms of 2D layers on metal surfaces may take different routes depending on metal substrate, precursor pressure, growth temperature and even the history of the substrate. For Ni layers and single crystals, the graphene growth becomes more complex due to the large solubility of carbon in the bulk Ni and the competing formation of surface carbides, Ni<sub>2</sub>C [114]. In this specific case, it is not possible with post-growth characterization methods to determine the contribution from the dissolved carbon and from the precursor. This problem was first approached *in situ* by Weatherup *et al.* [115] who studies the growth of a graphene layer as a function of exposure to C<sub>2</sub>H<sub>2</sub> with depth-resolved APXPS and *in situ* X-ray diffraction (XRD) for the study of graphene growth on polycrystalline Ni foil. Exposing a 600 °C hot Ni foil to an atmosphere of  $10^{-5}$  Torr C<sub>2</sub>H<sub>4</sub> led to the evolution of the C 1s core level peak as shown in Figure 11.

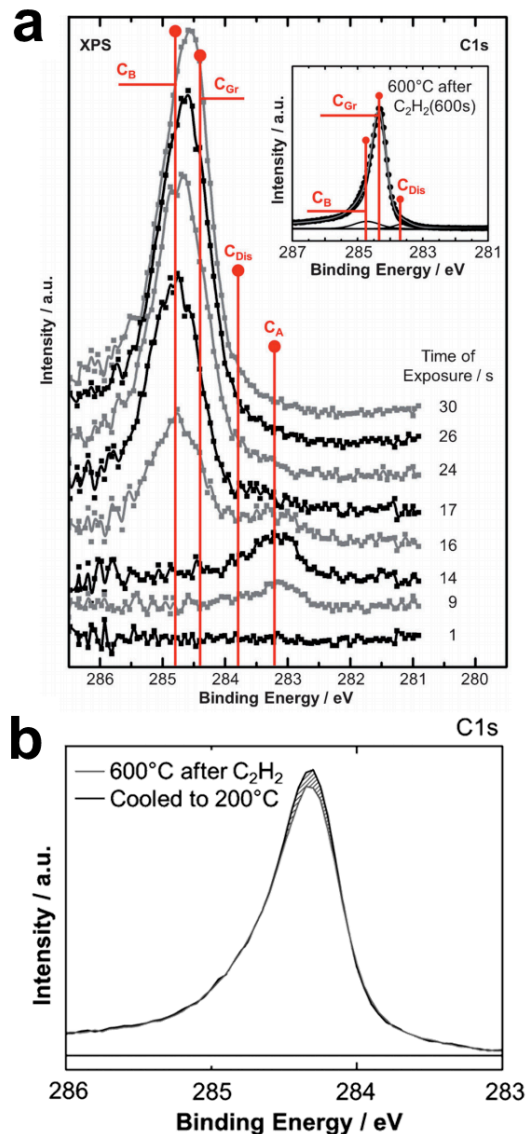


**Figure 11.** (a) APXPS C 1s core level spectra for a Ni (550 nm) film at 600 °C during CVD growth ( $C_2H_2$  approximately  $\sim 10^{-5}$  Torr). The spectra show the formation of graphene while the sample is hot and exposed to carbon precursors in the form of ethylene (isothermal growth). (b) C 1s core level spectra before and after 600 °C growth. A small increase of the total carbon intensity is observed due to precipitation of dissolved carbon to the surface. The main contribution to the graphene formation is by isothermal growth. Reproduced with permission from [115]. Copyright John Wiley & Sons. <http://dx.doi.org/10.1002/cphc.201101020>

In Figure 11, the  $C_A$  peak arises initially after  $C_2H_4$  exposure and corresponds to adsorbed carbon, from the decomposed precursor (ethylene). At increased exposure times, this carbon diffuses to the Ni subsurface forming a Ni-C alloy with carbon interstitially dissolved ( $C_{Dis}$ ). The latter structure was confirmed by XRD (not shown) verifying that no bulk carbide

was formed. After 16 s exposure, the C concentration has reached a level where graphene begins to grow, giving rise to the component  $C_{Gr}$  accompanied by the component  $C_B$ , which is attributed to  $sp^3$  carbon in defects and at edges at the graphene domains. The inset shows a C 1s spectrum after the precursor gas was evacuated subsequent to a 600 s exposure. The formation of the graphene clearly takes place isothermally to the growth temperature (Figure 11a) and the C 1s spectrum after cooling (Figure 11b) shows only a minor increase in the carbon concentration, which is then attributed to precipitation from the Ni-C solid solution [115]. The contribution to the graphene growth from subsurface carbon was found to increase at higher growth temperatures and yielded more disordered graphene layers. A lower temperature isothermal growth scheme was thus suggested for achieving higher quality graphene layers. This is an important result for optimizing the growth procedures and could not have been obtained by studying the system with conventional XPS. A similar behavior was observed for graphene grown at various temperatures on a clean Ni(111) crystal as well as on crystals with various amounts of initial subsurface carbon impurities [116].

During CVD growth of a 2D layer, the typical pressures used vary between approximately  $10^{-8} - 10^{-5}$  Torr. At this range, the gas cleanness plays a minor role compared to higher pressure studies. However, the APXPS results provide a signature of the graphene quality, which is averaged over the spatial range of the X-ray beam spot size and usually leaves out information about low density defects and rotational disorder. To obtain detailed information on the atomic scale, we suggest the complementary use of STM or AFM, and PEEM may be useful for rotational alignment.

The role of subsurface carbon for the graphene-Ni(111) interface interactions was subsequently further explored using Monte Carlo simulations and APXPS [117]. When a Ni(111) single crystal sample was heated to 400 °C while exposed to  $C_2H_4$  at various pressures [117], the main growth mechanism was shown to be in-plane transformation of surface carbides,  $Ni_2C$ . The formed graphene layer was stable at pressures up to approximately  $\sim 10^{-3}$  Torr. When increasing the pressure to  $\sim 10^{-1}$  Torr, a large amount of carbon diffused through the graphene defects and boundaries into the Ni crystal. The increase of dissolved carbon led to a weakening of the graphene-Ni interactions, but also to the formation of several graphene layers, which was not observed for exposures at lower pressures at this temperature. In extension of this line of thought, it was shown by time resolved APXPS (vacuum annealing) that a thin Ni layer placed

on a solid carbon source, heated to 600 °C, produced an inhomogeneous, few-layer graphene on the upper Ni surface due to diffusion and precipitation of the carbon through the Ni layer [118]. A more homogenous monolayer graphene layer can be achieved when Al<sub>2</sub>O<sub>3</sub> is introduced between the solid carbon source and the Ni layer [118]. Another approach for achieving a uniform graphene layer on polycrystalline Ni is to decorate the reactive Ni surface sites with Au, thus decreasing the available nucleation sites for the graphene [119]. The above are examples showing that the graphene-Ni interfacial interplay is complex and a small change in growth parameters may alter the final product tremendously.

Cu shows a huge potential for catalyzing graphene growth at industrial scales, and large-scaled growth by a roll-to-roll procedure is already applied [120]. The interaction between graphene and Cu is much weaker than the above-mentioned case of the graphene/Ni (gr/Ni) system, allowing the possibility of decoupling the graphene sheet from the Cu and transferring it to another substrate [85,121]. There exists a large body of publications characterizing the gr/Cu system by XPS, often where the samples are grown in a dedicated growth chamber and subsequently transferred through air to the XPS analysis chamber. For these *ex situ* XPS measurements, the reported XPS results differ, however, from those obtained by APXPS measurements. Kidambi *et al.* [122] reported on the APXPS study of graphene on polycrystalline Cu foil. The low solubility of C in Cu limits the growth to occur mainly by deposited precursors. No carbide is observed and the overall growth mechanism appears to be simpler compared to the case of Ni. A somewhat large charge transfer from Cu to graphene (n-doping) leads to a shift of the sp<sup>2</sup> graphene signature in the C 1s core level towards higher binding energy compared to other systems. The resulting sp<sup>2</sup> component was thus found at 284.75 eV [122]. In contrast, the sp<sup>2</sup> carbon binding energy is at 284.4 eV in some *ex situ* XPS studies [123]. The difference appears to be due to intercalation of O<sub>2</sub> for air exposed samples, or when O<sub>2</sub> is present in the residual atmosphere in a UHV setup, which consequently weakens the graphene-Cu interactions [122]. In such cases, where a contaminant is of high enough concentration to be detected, such as the O<sub>2</sub> intercalation layer, *in situ* APXPS during growth provides an advantage of pinpointing when during the growth process the contamination occurs. This provides extremely important information for optimizing a growth process.

The advantages and limitations of APXPS also apply to studying the growth of 2D layers other than graphene. The growth of hexagonal boron nitride (h-BN) on polycrystalline Cu was

studied by APXPS by Kidambi *et al.* [124]. The growth mechanism was found to be similar to that of graphene on Cu, i.e. isothermal direct growth but at  $\sim 975$  °C. However, interestingly, boron was observed to dissolve into the Cu subsurface layers forming a precursor for a highly reactive surface when the system was exposed to air and subsequently annealed. When heating was applied to the air exposed sample, the intercalated oxygen reacted with the dissolved boron, creating volatile boron-oxide species and effectively destroying the h-BN sheet.

### *Intercalation of Small Molecules*

Intercalation of species into substrate-2D layer interfaces has received much attention recently due to the prospects of gaining control of electronic, optical, mechanical, and chemical properties of 2D layers. The mechanism for intercalation depends on the type of 2D layer, substrate, and intercalated species as discussed above, but generally proceeds through defects and grain boundaries. The 2D layer decouples from the substrate through the formation of an interface layer and the energy cost to generate the decoupled 2D sheet must be compensated by energy gained through the adsorption of the intercalated molecule to the substrate.

Some fingerprints of intercalation are easily detected in XPS; for instance, the C 1s core level signature for graphene is usually shifted to lower binding energy upon intercalation, as described in the previous section for gr/Cu. Intercalation of h-BN has also shown a negative shift in binding energy for the N 1s and B 1s core levels. Additionally, the metal surface core level peaks are modified upon adsorption of intercalated molecules or atoms. In many cases it is beneficial to compare the adsorption structure below the 2D layer cover to that of the bare metal surface exposed to the same high-pressure gas using APXPS. A summary of all APXPS intercalation studies of 2D layers on transition metal surfaces, known by the authors to date, is summarized later in Table 1. A few cases are discussed in more detail in the following.

In general, it is found in several of the studies discussed in the following that the adsorption energy of a molecule or atom, when adsorbed on a metal surface below a 2D layer, is decreased as compared to the adsorption on the bare metal surface. This is due to the energy cost required to decouple the 2D sheet from the metal surface, which destabilizes the adsorbate. The adsorption energy reduction is for example observed for H<sub>2</sub> and CO intercalating between graphene and h-BN on Pt(111) [125-128]. In the case of CO, this effect turns out to be beneficial for an efficient CO oxidation at the metal-2D layer interface.

### *CO Intercalation*

In 2D layer/metal systems, the coverage of the intercalated CO needs to meet a threshold in order to overcome the initial barrier for decoupling the 2D layer. The threshold coverage thus scales with the interaction at the interface and can, for highly interacting systems, be reached by exposure to a higher pressure. Such a threshold is easiest to explore by gradually increasing the pressure until intercalation is observed. For spectroscopic investigation which requires both high pressure and fast data acquisitions, APXPS is a fitting technique. CO was found to intercalate a full layer of graphene on Pt(111) at pressures above approximately  $\sim 0.01$  Torr [125], while pressures above  $\sim 0.1$  Torr CO were needed to intercalate a 0.9 monolayer (ML) graphene layer on Ir(111) [129]. The CO configuration at the gr/Ir(111) interface was found to be similar to that found on a clean Ir(111) [129]. When decreasing the partial CO pressure back to UHV conditions, the CO desorbed from the bare Ir(111) surface, leaving a stable but lower coverage structure at the surface. This UHV related structure, conversely, did not form in the presence of a graphene cover. The study thereby confirms the existence of a CO pressure gap induced by the interface, which may be utilized for future pressure switching applications [129]. For future studies, it would be interesting to investigate whether similar defect effects, such as the sheet opening upon attachment of hydroxyl groups to the graphene edges [102], are at play. Due to the sensitivity limitations, such effects may be nearly impossible to detect using APXPS unless working with very small flakes of graphene where the concentration of edge-sites is increased. However, having a system of small graphene flakes could change the mechanism of intercalation entirely.

A comparison between CO intercalation below gr/Ni(111) and CO interaction with a Ni<sub>2</sub>C surface carbide on Ni(111) was performed by Wei *et al.* by APXPS [130]. A pressure-independent low coverage of adsorbed CO on Ni<sub>2</sub>C/Ni(111) was found in the ranges  $10^{-6}$  - 0.1 Torr. CO exposures to gr/Ni(111) led to a partial intercalation at  $p_{\text{CO}} > 0.1$  Torr and intercalation of a full CO layer at 5 Torr. The complete interlayer of CO led to a decoupling of the graphene from the Ni(111) surface. While the intercalated CO coverage at saturation was found to be similar to that of a bare Ni(111) surface, the graphene cover tends to suppress the binding of CO to Ni top sites in favor to the bridge sites. Partial removal of intercalated CO took place rapidly

between 80 °C - 100 °C. Removal of residual trapped CO could be achieved by annealing the sample to 200 °C [130].

The strongest graphene-metal interaction was observed for gr/Ru [131]. A gr/Ru(0001) system was studied by APXPS while exposed to CO [132]. The graphene layer on Ru(0001) is highly corrugated and the C 1s splits into two peaks separated by ~0.6 eV, corresponding to graphene areas strongly interacting with Ru (C1) and areas with weaker interaction (C2). The spectrum for the full ML graphene on Ru(0001) is shown in Figure 12 before CO exposure (bottom spectrum). The C 1s spectrum is complex due to overlapping Ru 3d peaks. Despite the complexity, a new C 1s component (C3) representing decoupled graphene is revealed after exposure to 1 Torr of CO. The system becomes fully intercalated after a prolonged (1 hour) CO exposure at a pressure of 10 Torr as shown in the top spectrum of Figure 12. Similar to the Ni case, the bridge sites become favorable adsorption sites for the intercalated CO.

The partial pressure of CO required for intercalation increases with the interaction strength between the graphene and the transition metal substrate. Since the adsorption energy of CO does not differ significantly for the transition metals of interest, the varying CO pressure necessary for obtaining saturated coverage in different systems may be related to the strength of graphene-metal interaction as also discussed in ref. [132]. The trend is summarized in Figure 13.



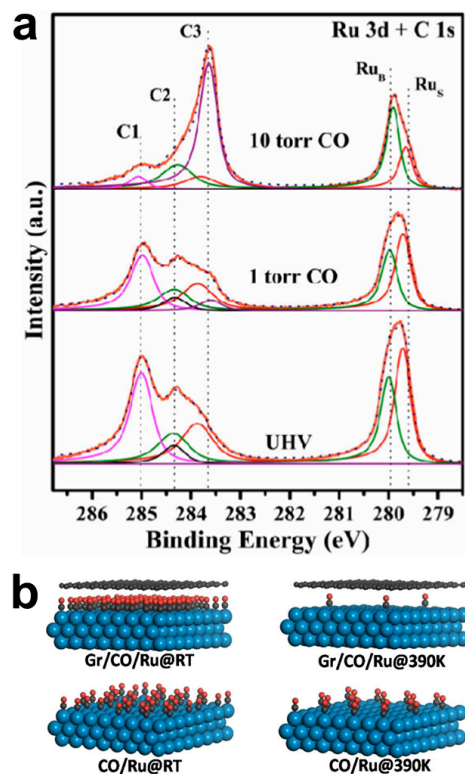


**Figure 12.** (a) C 1s and Ru 3d core level spectra obtained from a graphene covered Ru(0001) sample before and during exposure to high-pressure CO. (b) A sketch showing the surface CO coverage in 4 different situations: With and without graphene during a 10 Torr CO exposure (left) and the Ru sample with and without graphene after the 10 Torr exposure and a subsequent return to UHV (right). Reprinted with permission from Jin *et al. J. Phys. Chem. C*, 2014, **118**, 12391-8. [132] Copyright 2014 American Chemical Society.

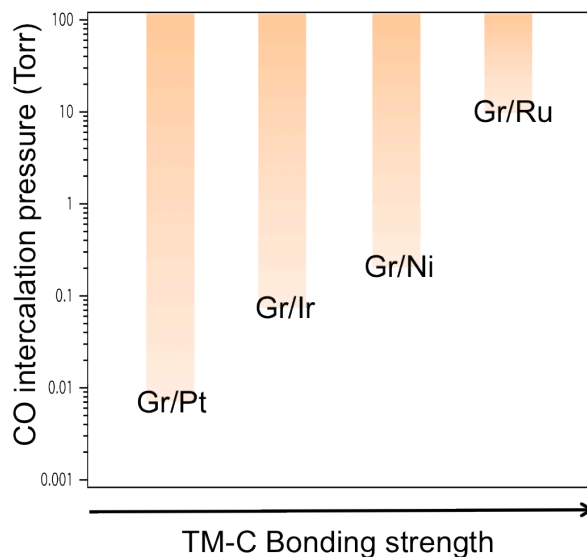


**Figure 13.** Schematic illustration of the CO intercalation pressure at various graphene-transition metal interfaces. Inspired by [132].

Similarly, intercalation of CO between h-BN and its metal substrate leads to a decoupling of the h-BN layer. CO intercalation was reported for h-BN on Rh(111) (h-BN/Rh(111)) [100] and h-BN/Pt(111) [127]. CO intercalation of gr/Rh(111) has not been reported in literature, but the interfacial interaction strength is similar to that of gr/Ru [133,134]. While the graphene-substrate interaction goes as  $gr/Rh > gr/Pt$ , the interaction of h-BN/Pt(111) appears to be stronger than that of h-BN/Rh(111). This statement is based on the APXPS results of the intercalation of CO in the two cases: CO intercalates the full monolayer (ML) at the h-BN/Rh(111) interface at  $p_{CO}$  0.01 Torr at room temperature, while  $p_{CO} > 0.1$  Torr is needed for intercalation of a full ML h-BN/Pt(111). The difference between the gr/CO/Pt(111) and h-BN/CO/Pt(111) interfaces is additionally reflected in the desorption kinetics, where CO desorbs already at room temperature from the latter system under UHV conditions [127]. This difference between the behavior of CO intercalation under graphene and h-BN may be explained by the polar nature of the h-BN sheet, yielding the stronger interaction to the metal than the nonpolar graphene [127]. Removal of CO and a recovery of the as-grown h-BN layer on Rh(111) occurs only when heating above 350 °C [100], indicating that the interaction of h-BN/Rh(111) is weaker than that of h-BN/Pt(111). The h-BN/Rh(111) system was also exposed to H<sub>2</sub>, H<sub>2</sub>O, O<sub>2</sub> and a mix of CO and O<sub>2</sub>, but only intercalation of CO under the reported conditions was observed [100]. As a side note, H<sub>2</sub> was

observed to intercalate under graphene on Ir(111) as measured by conventional XPS [135] and under graphene and h-BN on Pt(111) at 0.1 Torr measured by APXPS [128].

The interaction of h-BN with some transition metal surfaces (TMs) goes in the order of Ni > Ru > Cu > Rh as calculated in Ref [136]. From the above discussion the h-BN on Pt(111) should be placed on the left side of Rh in the scheme. Thus, APXPS provides a direct probe for the qualitative interaction strength between a 2D layer and its substrate through ambient-pressure CO intercalation. It will be interesting to see if CO intercalation on h-BN/TMs systems follows the same qualitative trend as for gr/TMs.

### *Intercalation of O<sub>2</sub>*

Oxygen intercalation has been widely studied for graphene on metal substrates under UHV conditions [92,137]. For oxygen intercalation to occur in the low-pressure range, a thermal activation above 225 °C for gr/Ir(111) [92] is needed. At room temperature, oxygen intercalation was however reported to occur on gr/Cu in ambient environments [138]. An additional parameter to consider when dealing with high pressures of oxygen in the presence of graphene is etching. This process happens at temperatures that depend on the pressure of the oxygen atmosphere, e.g. for graphene flakes on Cu foil: 500 °C at  $p_{O_2}$  approximately  $\sim 4 \times 10^{-5}$  Torr, 450 °C at  $p_{O_2} \sim 4 \times 10^{-2}$  Torr and 280 °C at  $p_{O_2} \sim 0.2$  Torr [138]. Oxygen intercalation was studied by APXPS for graphene flakes on polycrystalline Cu [138] and graphene on Ru(0001) [139,140] and for h-BN on Ru(0001) [140] and on Pt(111) [141]. For gr/Ru(0001) the intercalation occurred when heating the system above 150 °C in an oxygen atmosphere of  $p_{O_2}$  0.5 Torr [139], while heating to 200 °C is needed at 0.1 Torr or above 300 °C at a much lower oxygen pressure of  $5 \times 10^{-8}$  Torr for 0.5 ML graphene [140]. A bare Ru(0001) oxidizes readily at room temperature when exposed to 0.5 Torr oxygen [139]. To reverse the oxidation of a clean Ru(0001) substrate, temperatures of around 1000 °C are required. In contrast, oxygen desorbs from the gr/Ru(0001) interface already at 420–470 °C [139]. This temperature again confirms that the adsorption energy of the intercalated species below the graphene cover is decreased by the additional energy cost required for decoupling the graphene. For a full ML h-BN on Pt(111), oxygen intercalation occurs at an oxygen pressure of 0.1 Torr when the sample is heated above 200 °C. Keeping this temperature and returning to UHV does not change the XPS signature for oxygen intercalated h-BN/Pt(111), as the desorption occurs when annealing the sample above 300 °C [141].

On a final remark, CO intercalation was reported to occur at  $10^{-6}$  Torr when the sample was *already* intercalated by oxygen and kept at 200 °C, while approximately  $\sim 0.1$  Torr was needed to intercalate an “empty” h-BN/Pt(111) interface [141]. This co-intercalation resulted in the removal of intercalated oxygen by CO<sub>2</sub> formation below the h-BN cover, similar to what has been observed for graphene confinement induced reactions [125,126].

The examples discussed in this section point towards the direction of many of the future investigations in this field of 2D-layer/solid interfaces, where co-adsorption and reaction in the confined space between a 2D material and a metal substrate may lead to new reaction pathways and products. APXPS is an excellent method to study the chemical and electronic properties of the substrate, 2D film, and the adsorbed species as the reaction occurs. As we have discussed in detail, the limited sensitivity of APXPS in detecting low concentrations of defect states and/or impurities is perhaps the most prominent disadvantage of application of this technique to such 2D layer systems, however this can be compensated for somewhat by judicious application of other complementary *in situ* surface characterization methods.

We now turn our attention to another condensed phase/vapor interface, namely the liquid/vapor interface, which poses its own challenges for surface science studies.

System	Coverage	Gas	Pressure (Torr)	Outcome	T	Core level shifts (eV)			Reference
						C1s	N1s	B1s	
gr/Ni(111)	1 ML	CO	>0.1	Intercalation	RT	-1.1	-	-	[130]
h-BN/Rh(111)	1 ML	CO	0.075-0.15	Intercalation	RT	-	-2.5	-2	[100]
gr/Ir(111)	0.5 ML	CO	0.075	Intercalation	RT-520 K	-0.3	-	-	[129]
gr/Ru(0001)	1 ML	CO	10	Intercalation	RT	-1.36, -0.71	-	-	[132]
h-BN/Pt(111)	0.5 ML	CO	$1 \times 10^{-5}$	Intercalation	RT	-	-0.3	-0.3	[127]
h-BN/Pt(111)	1 ML	CO	0.1-0.5	Intercalation	RT	-	-0.3	-0.3	[127]
h-BN/Pt(111)	1 ML	CO	0.1	Intercalation	RT	-	-0.3	-0.3	[141]
gr/Pt(111)	1 ML	CO	0.01	Intercalation	RT	-0.2	-	-	[125]
gr/Pt(111)	1 ML	O <sub>2</sub>	0.1	Intercalation	>373 k	-0.2	-	-	[125]
h-BN/Ru(0001)	1 ML	O <sub>2</sub>	0.1	Intercalation	RT	-	-2.44	-1.88	[140]
gr/Ru(0001)	1 ML	O <sub>2</sub>	0.1	Intercalation	200 C	-1.39, -0.67	-	-	[140]
gr/Ru(0001)	1 ML	O <sub>2</sub>	0.5	Intercalation	150 C	-1.36	-	-	[139]
gr/Cu foil	Flakes	O <sub>2</sub>	$3.75 \times 10^{-5}$	Intercalation	180-280 C	-0.35	-	-	[138]
gr/Cu foil	Flakes	O <sub>2</sub>	$3.75 \times 10^{-5}$	Etching	>500 C	-0.35	-	-	[138]
gr/Cu foil	Flakes	O <sub>2</sub>	$3.75 \times 10^{-2}$	Intercalation	180-280 C	-0.35	-	-	[138]
gr/Cu foil	Flakes	O <sub>2</sub>	$3.75 \times 10^{-2}$	Etching	>450 C	-0.35	-	-	[138]
gr/Cu foil	Flakes	O <sub>2</sub>	0.15	Intercalation	180-280 C	-0.35	-	-	[138]
gr/Cu foil	Flakes	O <sub>2</sub>	0.15	Etching	>280 C	-0.35	-	-	[138]
h-BN/Pt(111)	1 ML	O <sub>2</sub>	0.1	Intercalation	RT	-	-0.6	-	[127]
h-BN/Pt(111)	1 ML	O <sub>2</sub>	0.1	Intercalation	200 C	-	-0.6	-0.4	[141]
gr/Pt(111)	1 ML	H <sub>2</sub>	0.1	Intercalation	RT	-0.1	-	-	[128]
h-BN/Pt(111)	1 ML	H <sub>2</sub>	0.1	Intercalation	RT	-	-0.1	-0.1	[128]

**Table 1:** Summary of all intercalation studies of 2D layer/metal substrate interfaces by APXPS reported to date (July 2016)

## Liquid/Vapor Interfaces

### *General Considerations*

Liquid/vapor interfaces play an important role in many natural and technological processes. In nature, liquid aerosols host reactions that are important for atmospheric chemistry [142,143]. Basic processes (such as CO<sub>2</sub> uptake) taking place at the surfaces of liquid masses (oceans, seas and lakes) are critical for the global climate and the local concentration of trace gases in the atmosphere. In chemical engineering, many unit operations (e.g. absorption, stripping) and some types of reactors (e.g. trickle bed) involve mass transfer between a liquid and a gas phase. Thus the liquid/vapor interface is of critical importance for the efficiency of these operations. Finally, combustion of liquid fuels is a complex process and the liquid/vapor interface also plays a major role.

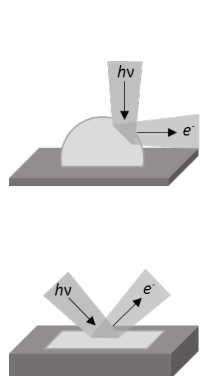
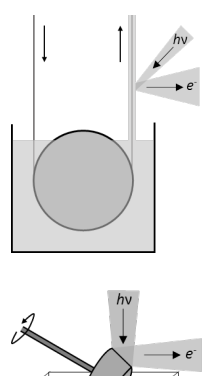
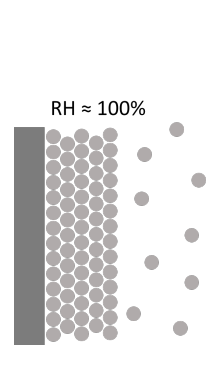
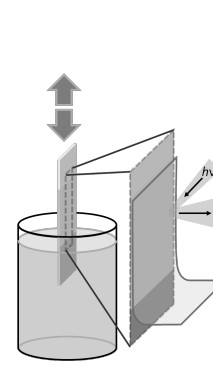
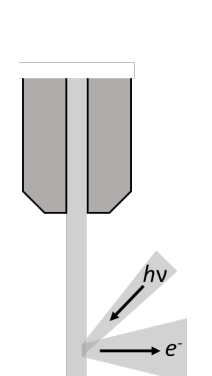
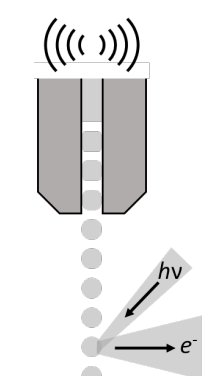
With the development of APXPS, studying samples under ambient gas pressure has become a routine practice. Aqueous solutions at room temperature in equilibrium with their vapor (~20 Torr) have also been studied routinely in recent years [144-146]. The obvious scientific relevance and importance of water aside, it is a technically less challenging sample for APXPS than most others since the electron scattering of the gas phase is relatively low because water only contains three atoms, and only one of them (oxygen) is a relatively strong electron scatterer. As the number of atoms in a molecule increases, the electron scattering at a given pressure becomes stronger.)

Some common techniques for preparing liquid surfaces for XPS analysis are illustrated in Figure 14. The preparation and measurement of liquid sample surfaces is challenging for a number of reasons:

- 1) The background vapor pressure needs, in many cases, to be maintained at the equilibrium pressure for the given liquid temperature to avoid excessive consumption of liquid phase, as well as changes in liquid temperature and concentration of soluble species.
- 2) Many technologically important liquids, such as water and hydrocarbons, are good electrical conductors, and photoemission will cause electrical charging of the surface [147].
- 3) Due to the high diffusion rate in liquids, their surfaces are particularly susceptible to contamination since even small amounts of contaminants can migrate quickly to the interface.

- 4) Most liquids are molecular compounds, which are susceptible to damage by the X-ray beam.
- 5) Typical solutes (which have concentrations in the mole/L range or less) give only small XPS signals so low that long acquisition times are necessary.

While the development of APXPS has been a milestone in making XPS routinely accessible at Torr pressures, other technical advances to overcome the obstacles for the preparation of liquid interfaces will be discussed next.

	Static drop	Continuously wetted surface	Condensation	Meniscus (dip & pull)	Liquid jet	Droplet train
<b>Configuration</b>						
<b>Working pressure / evaporation</b>	Equilibrium vapor pressure / minimal evaporation	Equilibrium vapor pressure / minimal evaporation	Equilibrium vapor pressure / minimal evaporation	Equilibrium vapor pressure / minimal evaporation	Equilibrium vapor pressure/minimal evaporation <b>OR</b> high vacuum/strong evaporation	Equilibrium vapor pressure/minimal evaporation <b>OR</b> high vacuum/strong evaporation
<b>Charging</b>	Thick liquid film might charge depending on conductance of solution	Thin liquid film grounded through substrate	Thin liquid film grounded through substrate	Thin liquid film grounded through substrate	Minimal charging through short exposure to X-rays	Minimal charging through short exposure to X-rays
<b>Surface cleanliness</b>	Contamination increases with time	Less contamination due to constant formation of a new surface	Contamination increases with time	Contamination increases with time	Contamination free due to rapid formation of new surface	Contamination free due to rapid formation of new surface



## ***Sample Preparation Techniques***

### *Liquid Jets*

A liquid jet is formed by forcing a liquid through a small orifice using high pressure (~100 bar [148]). Liquid jets can be formed in the laminar regime but they spontaneously break apart into droplets after a critical length due to Plateau-Rayleigh instability. Because of this critical length, XPS measurements on a liquid jet have to be performed near the capillary exit where the jet is still cylindrical and smooth.

The constantly refreshed sample volume (and surface) in a liquid jet provides several advantages. Typical jet velocities are in the range of tens of meters per second, and the surface is probed within a few mm after exiting the orifice/capillary. Thus, the surface is always clean as they are formed less than a millisecond before analysis. Secondly, charging and beam damage are negligible since the surface is only exposed to the X-ray beam for typically a few tens of microseconds. Jets have been used for the investigation of liquid surfaces at Siegbahn in the early days of APXPS, but only a single study using this method was published at that time [17].

In 1997 Faubel *et al.* demonstrated that a liquid water jet of ~10  $\mu\text{m}$  diameter could be produced in a vacuum chamber, maintaining a chamber pressure of better than  $10^{-5}$  Torr using a vacuum pump speed of 3000  $\text{L s}^{-1}$  [148]. Their setup allowed ultraviolet photoelectron spectroscopy to be applied to technically challenging liquids such as water (high vapor pressure) and *n*-nonane (high vapor pressure and extremely low conductivity,  $\sigma < 10^{-12} \Omega^{-1} \text{cm}^{-1}$ ). In the last decade, microjet setups have also been used by several other groups in the last decade for photoelectron spectroscopy or X-ray absorption experiments [149-152].

One disadvantage of liquid jets is the need for a constant supply of the sample (unless it is recirculated), which may be a problem if the liquid is expensive or scarce. Another issue, which is more prominent in non-conducting liquids, is the so-called streaming current effect. This phenomenon results because charge from the electrical double layer at the capillary/capillary-liquid interface is swept away with the jet. It causes the jet to charge significantly and thus shifts photoelectron peaks. Faubel *et al.* observed this charge to be spatially uniform, only causing a fixed shift of the peaks and no broadening [148]. Liquid jet chambers are typically pumped to an extent that the pressure is lower than the vapor pressure of the liquid at room temperature. The pumping speed over a liquid jet determines the pressure around it. If the jet has enough time

equilibrate with this vapor, it reaches the equilibrium temperature at this pressure. The temperature of the jet, and thus the liquid under investigation, can be varied by changing the pumping speed and the distance at which the jet surface is measured after leaving the orifice [152].

### *Droplet Train*

In atmospheric science, droplet trains have been used to measure the gas uptake of liquid aerosols [153,154]. A typical setup is very similar to a liquid jet device, only that the orifice is not static but can be vibrated at appropriate frequencies (typically several tens of kHz) to break up the liquid jet into droplets of well-defined size and droplet separation. In 2008, Starr *et al.* demonstrated that a droplet train system can be used in an APXPS experiment to measure the surface propensity of methanol in an aqueous solution. Droplet trains have the advantage over liquid jets that they are stable over longer distances (up to 40 cm for  $p < 40$  Torr [154] and  $\sim 1$  m for  $p < 20$  Torr [59]). This stability allows the exposure time of the liquid to the gas to be varied over a greater time (up to tens of milliseconds) than in the case of the liquid jet (sub-milliseconds). At such timescales, the thermal equilibration between the liquid surface and the vapor is complete, which means the temperature of the droplet surface can be manipulated by changing the background vapor pressure in the chamber [152].

### *Static Droplets*

Static droplets can be studied with standard XPS if the vapor pressure of the liquid in question is in the high vacuum range. Ionic liquids are an example for this case [155,156]. Almost all other liquids have vapor pressures that are incompatible with UHV near room temperature. Static drops have several disadvantages, such as contaminant accumulation on the surface, charging (if the liquid and solid support are not conductive enough), and possibly beam damage. On the positive side, static droplets offer the advantage that liquid surfaces can be measured for hours or days if the equilibrium vapor pressure is maintained in the experimental cell, allowing measurements of slow vapor/liquid reactions. Static droplets can also be prepared in acoustic or optical traps [157,158] where they are suspended without mechanical support and thus electrical connection, which will in most cases lead to severe charging problems. To date, no APXPS studies on static droplets have been reported.

### *Vapor Condensation*

Liquid layers can be condensed on solid substrates if the pressure of the vapor is near the saturation vapor pressure of its liquid at the temperature of the substrate and the substrate favors adsorption from the gas phase, i.e. in the case of water vapor, a hydrophilic substrate. Liquid water films with thicknesses exceeding a few layers can be grown at above ~90% relative humidity (RH) [159]. At and above 100% RH, condensation and thus layer growth proceeds indefinitely, leading to a constant spatial change of the position of the liquid surface which hampers the APXPS measurements.

Condensation of water on a soluble solid, like an alkali halide salt, creates a saturated solution above the deliquescence relative humidity, (e.g., 75% for NaCl), which can be studied with APXPS [160-164].

### *Dip-and-Pull/Meniscus Method*

Liquid layers with thicknesses in the range of 10-20 nm can be prepared using the so-called “dip-and-pull” [144] (or “meniscus” [165]) method. In this method, a solid plate/foil is partly immersed into a liquid reservoir and pulled out slowly (at a rate of  $\sim\text{mm min}^{-1}$ ), forming a thin liquid layer. This nm-thick liquid layer typically extends a few cm above the macroscopic meniscus that forms near the liquid reservoir, while the macroscopic meniscus itself extends only a few mm above the liquid. This thin liquid layer is stable in the presence of the near-saturation vapor pressure of the liquid (in the case of water, RH  $\sim$ 100%).

### *Dynamic Wetting Methods*

In the pioneering APXPS work on liquids by Siegbahn *et al.*, clean liquid surfaces were created by dynamic wetting of a moving surface, such as that of a wire, disk, or trundle [166-169]. The wire setup had the advantage over the liquid jet technique at the time because the position of the liquid surface could be controlled better. This technique allowed scans over extended periods of time (many hours), which is necessary to study solutes since their concentrations are generally low. The main advantages of the disk and trundle setups is that they enable cooling of liquids under investigation (important for liquids with high vapor pressure), as

well as changing the detection angle of electrons in a controlled way for depth-dependent measurements using a (fixed energy) laboratory X-ray source.

### *Ice Surfaces*

A special case for a liquid/vapor interface is that of the liquid-like layer on ice [170]. As on most solids, a premelted layer forms at the ice surface at temperatures close to the melting point. For the investigation of the liquid-like layer, a bulk ice sample has to be grown first, for instance by using a thermoelectric (Peltier) sample holder, as discussed in the previous section [58]. The ice sample has to be maintained at 100% RH, lest it will either continue to grow or evaporate – precise temperature and pressure control are paramount in these experiments.

### ***Binding Energy Referencing for Liquid Samples***

In photoelectron spectroscopy the binding energies for a gas are commonly referenced to the vacuum level at infinity, whereas the binding energy for a solid are referenced to the Fermi level [171]. Liquids make an interesting case – a conductive liquid (such as a liquid metal) would have its Fermi level aligned with a conductive solid substrate if they are in electrical contact. That case requires no different treatment than that of a solid sample, i.e. BEs are referenced to the Fermi energy. However, many liquids are non-conductors without a well-defined Fermi level; while the binding energy scale of the liquid spectrum can in practice be referenced to the Fermi level by measuring e.g. a clean metal foil, the vacuum level of the liquid is in most cases a more appropriate choice for binding energy referencing. This also makes comparing binding energies with those of the gas phase (which is fundamentally interesting) straightforward.

A detailed treatment of BE referencing can be found in the work of Siegbahn et al. [172] for the case of a liquid in contact with a metal. The procedure will not be explained in detail here, but briefly it involves: i) measurement of a gas with a known BE mixed into the gas phase (this also provides the information to calibrate the BE for the vapor and other gases above the liquid), ii) estimation of the Volta potential ( $\Phi_{Volta}$ ) between the analyzer entrance and the liquid surface, and iii) finding the constant “k” ( $0 < k < 1$ ) that is a function of the experimental configuration.

Parts ii and iii in the procedure highlight the fact that for the gas phase above a liquid, the vacuum level is a function of position between the liquid surface and the entrance aperture to the electrostatic lens system, i.e. the two closest surfaces of the gas phase volume from which

electrons are detected by the spectrometer (see Figure 19 below). The vacuum levels of the liquid or solid sample and the entrance aperture are in general not aligned, which leads to a gradient of the vacuum level in the space between sample and aperture (i.e. Volta potential). Since the gas signal originates from a finite volume, this gradient leads to broadening of the gas phase peaks. The average value of the vacuum level is  $E_F + \Phi_{ana} + k\Phi_{Volta}$  [172]. In many cases though, the main interest is not the absolute BE but rather the changes in the BE of the liquid versus the gas; thus all photoelectron peaks in the system are referenced to the same binding energy scale.

Sample charging due to photoionization is not a problem for gases and conducting liquids such as ionic solutions, but the binding energy scale must be corrected for charging in the case of non-conducting liquids, which is generally not trivial. In the case of liquid jets, Faubel *et al.* show charging due to photoemission is negligible [148]. However, charging due to the so-called streaming current can be quite significant (on the order of tens of volts). Calculating the surface voltage due to streaming current is relatively straightforward as long as the current is known, and the current can be measured easily by electrically isolating the jet orifice. Charging in other experimental configurations is harder to quantify mainly due to difficulties in measuring the current that goes through the sample. Using an internal standard, i.e. a molecule with a known binding energy, is one way to mitigate this problem.

### ***Exemplary Cases***

In the following we discuss two examples for the application of APXPS to the measurement of liquid surfaces, in both cases those of aqueous solutions. Ghosal *et al.* studied the ion distribution at the vapor–liquid interface of two saturated alkali halide solutions, KBr and KI [173]. The study was the first direct, quantitative observation of the anion/cation ratio and absolute concentrations at the surface of an aqueous salt solution. The samples were prepared by exposing the freshly cleaved salts to water vapor (see Figure 14 – condensation method). Experiments were performed by keeping either the temperature (-10 °C) or pressure (2 Torr) constant, and varying the other parameter. Pressure and temperature were combined into relative humidity (%RH) scale according to:  $\%RH = 100 \times (P / P^{sat}(T))$  where  $P$  is the water vapor pressure during the measurement and  $P^{sat}(T)$  is the equilibrium vapor pressure of water at temperature  $T$ .

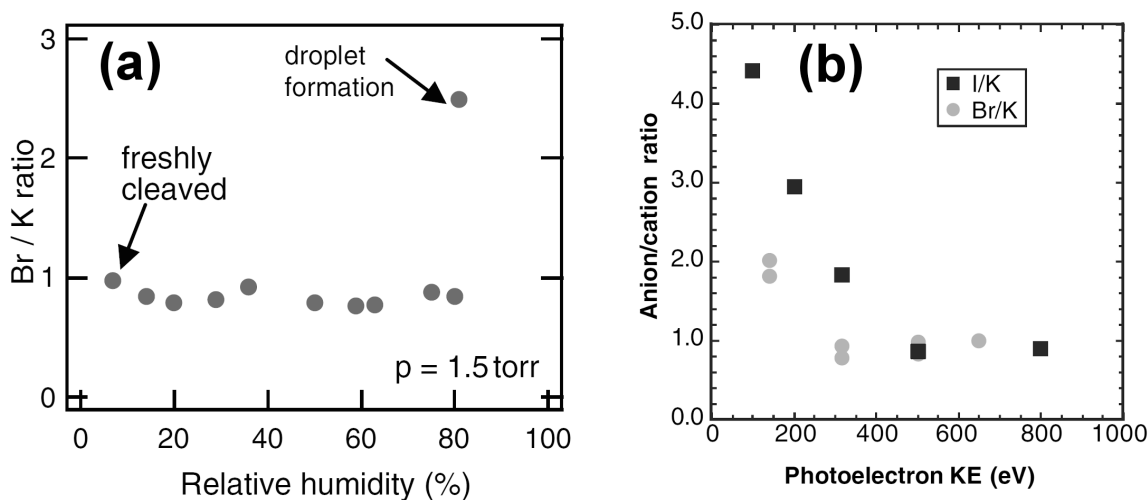


**Figure 15.** (a) Br/K atomic ratio, as calculated from APXPS data, of a KBr surface as a function of relative humidity at constant pressure (1.5 Torr). Photoelectron kinetic energy is 160 eV for both elements. (b) Anion/cation ratio for deliquesced KBr and KI as a function of the photoelectron kinetic energy used. From reference [173]. Reprinted with permission from AAAS. <http://dx.doi.org/10.1126/science.1106525>

Figure 15a shows the Br/K atomic ratio as a function of relative humidity for a freshly cleaved KBr sample. Up to  $\sim 80\%$  RH, the Br/K ratio is almost constant at the expected value of 1.0 for the solid salt. An abrupt increase in the Br/K ratio is observed at the deliquescence point of  $\sim 80\%$  RH. The photoelectron kinetic energy used for the experiment in Fig 11a was 160 eV, which means the signal originates mostly from the top atomic layers of the surface. Using a range of kinetic energies (by changing the photon energy) serves as a method for depth profiling. The anion/cation ratio for KBr and KI is shown in 11b as a function of photoelectron kinetic energy. For both KBr and KI, the ratio is greater than 1.0 at lower kinetic energies (i.e., near the surface) and close to 1.0 at higher kinetic energies (i.e., towards the bulk of the solution), further confirming the enhancement of large, more polarizable anions over cations at the interface, which was predicted from molecular dynamics simulations [174]. In addition to the relative concentrations, the absolute concentrations of  $\text{K}^+$ ,  $\text{Br}^-$ ,  $\text{I}^-$ , and  $\text{H}_2\text{O}$  were also estimated. In addition, it was found that the absolute concentrations of halides at the interface were also enhanced.

An inherent limitation in the study of samples prepared via this condensation method is the lack of control over the dissolved salt concentration – measurements are only possible for the

saturated salt solution. Depending on the system of interest, varying the concentration of dissolved ions may be desired.

The behavior of  $K^+$  and  $F^-$  at the liquid-vapor interface of aqueous KF was studied by Brown *et al.* using a liquid jet setup (see Figure 14 – liquid jet method) [150]. Instead of a deliquesced salt, a 6 M solution of KF was used. Although the liquid jet setup is suited for arbitrary solute concentrations, the signal from the solute is high enough only for concentrations greater than  $\sim 1$  M for practical purposes. It was found that F/K ratio was constant, within experimental sensitivity, as a function of photoelectron kinetic energy. The results were in agreement with molecular dynamics simulations [174,175]. The absence of adventitious carbon on the liquid-vapor interface demonstrated the strength of the liquid jet method for avoiding contamination.

The reaction of NaBr with ozone in the presence and absence of citric acid (a proxy for oxidized organic material on sea surfaces) was studied, including kinetic uptake measurements, with APXPS combined with a liquid jet [176]. Instead of using different photon energies for different core levels to get the same photoelectron kinetic energy, higher order components of a single photon energy (229 eV) – a product of the monochromator – were used (in this case, Br 3d, Na 2s, C 1s, and O 1s, see Figure 16a). 2<sup>nd</sup> order (458 eV) and 3<sup>rd</sup> order (687 eV) components were used to obtain C 1s and O 1s regions, respectively, shown in Figure 16a. A quantitative analysis based on photoemission cross sections and absolute concentrations was not made. Rather, trends in the relative signals of each component with respect to O 1s were calculated (Figure 16b). An increase in citric acid concentration correlated with a decrease in the Br/O ratio and an increase in the Na/O ratio at the surface. The lower surface concentration of  $Br^-$  was correlated with the faster uptake kinetics of  $O_3$  observed in the presence of citric acid.

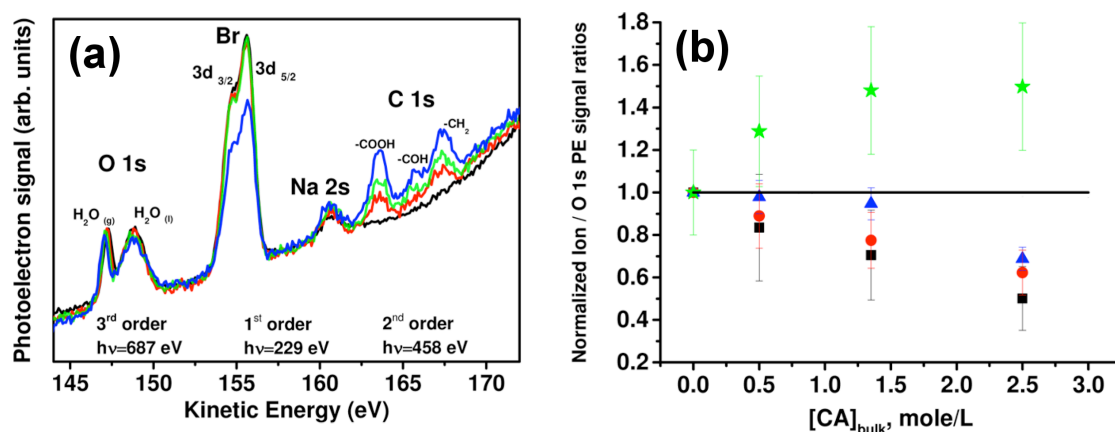


**Figure 16.** (a) Photoemission spectra from NaBr + citric acid (CA) solutions using a liquid jet setup in combination with APXPS. C 1s and O 1s signals are collected using the second and third order components of the main photon energy (229 eV), yielding similar photoelectron kinetic energies. Different colors are increasing CA concentrations (0.03, 0.06, and 0.12 M). (b) Relative peak intensities of Br 3d and Na 2s as a function of CA concentration: For Br 3d, 0.03 (squares), 0.06 (circles), and 0.12 M (triangles) NaBr concentrations. For Na 2s, only data for 0.12 M NaBr are shown (stars). The horizontal solid line illustrates the behavior expected for the bulk solution for reference. Reprinted with permission from Lee *et al.*, *J. Phys. Chem. A*, 2015, **119**, 4600-08 [176]. Copyright 2015 American Chemical Society.

While the liquid jet allows for flexibility in the solution concentration not afforded via the condensation method, there is a limit in the reaction timescales accessible when using this sample preparation technique. Because the liquid jet is flowing at speeds greater than meters per second, and thus the reaction time of the jet with the vapor phase before being measured by APXPS is on the order of milliseconds or less, reactions between the vapor/liquid phases occurring on timescales slower than are difficult to probe.

After discussing the APXPS measurements on liquid/vapor interfaces we now turn to the investigation of liquid/solid interfaces, arguably the most challenging interface to explore with APXPS or other interface sensitive spectroscopies.



## **Solid/Liquid Interfaces**

### ***General Considerations***

Understanding processes at solid/liquid interfaces is relevant in several fields including electrochemistry, heterogeneous catalysis, surface corrosion, geochemistry, and environmental chemistry. While the ability of XPS to quantify chemical and electronic changes in materials qualifies it as an appropriate technique to study the electronic structure of the liquid/solid interface, its inherent surface sensitivity remains an obstacle for widespread use of the technique. The small inelastic mean free path (IMFP) of electrons requires samples to have a thin liquid layer on a surface, thus complicating sample preparations. Using higher photon energies increases the IMFP of photoelectrons to allow a deeper probing depth; the tender X-ray region (2 to 7 keV) offers the ability to probe liquid layers less than 30 nm [144,177]. Even though a signal from a buried liquid/solid interface can be obtained, the majority of the signal originates from the bulk liquid and solid. Parsing the small interface contribution out of the total sample signal is a major reason the liquid/solid interface has been inaccessible by many techniques [178]. Despite this obstacle, it is possible to probe the liquid/solid interface. Combining the standing wave photoelectron spectroscopy technique with APXPS even offers precise depth profiling and will be discussed in more detail below.

Enabled by their low vapor pressures, UHV XPS has been used to study the interface between solid electrodes and ionic liquids [155,156]. A drop of ionic liquid on an angled substrate allowed for the preparation of a film thin enough to be probed by a laboratory X-ray source. APXPS offers the opportunity to use more volatile liquids, though more complex sample preparations are needed. There are four main techniques for sample preparation: condensation, the meniscus method, liquid jets, and liquid cell. These techniques are discussed in detail below, including limitations and future possibilities. Examples highlighting the capabilities of liquid/solid interfaces are presented at the end of this section.

### ***Sample Preparation Techniques***

#### ***Condensation***

The simplest method to prepare a thin layer of liquid on a solid is to increase the relative humidity in the analysis chamber to close to saturation (in the case of water, just below 100%

RH), where a photoemission signal from the molecular water indicates the condensation of a thin water film (see Figure 14). Depending on the thickness of the liquid layer, soft X-rays can probe the liquid/solid interface [161]. While water is the most frequently used liquid in this method, it is possible to use others. Thin films of solutions are prepared by the deliquescence, or rehydration, of salts or molecules that were *ex situ* deposited onto a substrate [161,179]. However, the inability to control the concentration or pH of the thin liquid films is a limitation of this technique. Additionally, adventitious carbon, a ubiquitous impurity, often increases in concentration at high humidity. Electrochemical control of the solid/liquid interface requiring reference electrodes in bulk solution is incompatible with this method. Thus, this liquid/solid interface preparation method is limited to a few special cases, such as studying the speciation of ions at the interface of very thin solution layers [179].

#### *Dip-and-pull/Meniscus Method*

A second method for generating a thin film on a substrate involves dipping the sample in a beaker of solution in the analysis chamber and slowly pulling the sample out of the liquid to extend the meniscus of the solution several millimeters along the sample surface, as discussed in the previous section. This technique, schematically depicted in Figure 14, is the dip-and-pull or meniscus method [144,146]. The beaker of solution allows for pH and concentration control. Placing counter and reference electrodes in the beaker offers electrochemical control; shifts in binding energies with changes in applied bias confirm that the thin film is in electrochemical contact with the bulk solution [144,146]. Depending on the electrochemical reaction being studied, there may be limitations to species diffusion or interference from gas bubble formation. Solution films prepared with this method are between 10 and 30 nm thick, requiring tender X-rays to probe the liquid/solid interface [144,177]. In addition to electrochemical experiments, pH and concentration dependent studies, hydrated biological systems, membranes, and corrosion processes are possible areas of inquiry for this method.

#### *Particles in Liquid Jets*

Passing a solution through a small capillary inside an analysis chamber can create a jet of liquid with a diameter with usually a few tens of  $\mu\text{m}$  (see Figure 14). As mentioned previously, liquid jets are often used to study liquid/vapor interfaces, but by adding nanoparticles to the

solution, the liquid/nanoparticle surface interface can be probed if a sufficient concentration of nanoparticles exists close to the liquid/vapor interface [149,180]. Liquid jets offer the advantages of concentration and pH control of an impurity-free liquid (even free from adventitious carbon) [181]. Constant refreshing of the sample in the photon beam typically prevents beam damage. Though soft X-rays have been successfully used to probe the liquid/nanoparticle interface [149,180,182,183], hard or tender X-rays would permit the study of nanoparticles that are farther from the liquid/vapor interface [181]. Recently, it has been shown that adding a pinhole to a synchrotron beamline can shape the beam to match the liquid jet diameter, thus reducing the overlapping gas phase signal of the solvent [184]. While no time-resolved studies of liquid jets have yet been conducted using APXPS, there is great potential in this area [181]. If a reaction is on the correct time scale, it could be initiated in the reservoir, gradually change the solution, and be followed with APXPS. One potential disadvantage of using liquid jets is the large amount of sample that is needed, especially nanoparticles that can be particularly expensive [181]. However, a continuous loop system that enables the trapped used solution to reenter the liquid jet reservoir would mitigate this issue.

### *Liquid Cells*

In the final sample preparation method, the liquid/solid interface is formed at a thin membrane which isolates a liquid in a cell from the analysis chamber. In this strategy, the photons and photoelectrons travel through the membrane layer to probe the interface, illustrated in Figure 17; this arrangement eliminates overlapping gas phase peaks, as there is no headspace above the liquid being probed by the X-rays. Solution concentrations and pH can both be accurately controlled. Depending on the cell configuration, the solvent could either be static or flowing behind the membrane, with electrochemical control possible in either situation. Though this method is currently the least developed, it offers several potential advantages. A robust, leak-tight liquid cell could be used in standard UHV instruments, greatly increasing the availability of the technique. Difficult samples, such as toxic, reactive, and/or radioactive materials, could be measured. Depending on the membrane strength, liquids and gas at much higher pressures could be accessed to bridge the pressure gap [185].

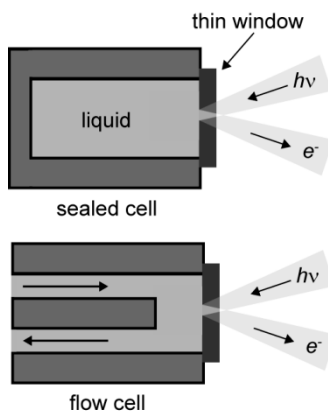


**Figure 17.** Schematic representation of two liquid cells to probe the solid/liquid interface. A thin window separates the liquid from the vacuum, is transparent to photons and photoelectrons, and acts as the solid of the probed interface. The top illustrates a cell where the liquid is sealed. In the flow cell in the bottom, the liquid is constantly refreshed at the interface.

The largest limitation of this method is the membrane material, which must be thin enough to be sufficiently transparent to photoelectrons yet thick enough to hold the pressure differential. Silica [186] and Nafion [187] require hard or tender X-rays [188] while graphene [42,189] and graphene oxide [189] allow liquid cell studies with soft X-rays. Since the window material is also the solid component of the interface, measurements are currently limited to interface studies of solid materials that can be fabricated into a thin window or deposited onto the windows, such as electrodeposited species [42] or thin films [186]. Depositing nanoparticles or using a solution of nanoparticles to probe the solution/nanoparticle interface is also feasible [188].

Other challenges need to be overcome to further advance this sample preparation technique. Window fabrication (in the case of etched Si) or transfer to the cell (in the case of graphene or graphene oxide) can introduce impurities [185]. Especially for static solutions, beam damage can lead to bubble formation, causing interference with the photoelectron signal and possibly window bursting [185]. Kraus and coworkers are developing a microchannel plate with many graphene windows to reduce the solution area exposed to the photon beam and prevent signal loss if a few windows burst [185]. Depending on the system studied, spectral features from the window material could interfere with peaks of interest, or the window material may participate in chemical reactions [186,188]. Though this sample preparation technique is still the least developed, it holds great promise to expand APXPS to a new set of users without

differentially pumped spectrometers and to a wide variety of traditionally difficult-to-probe samples.

## ***Exemplary Cases***

### *Nanoparticle/Liquid Interface*

By using a solution of nanoparticles in a liquid jet, the solid/liquid interface of the particles can be probed. Such a study was performed by Brown and coworkers [183] to investigate directly the effect of pH on the protonation and deprotonation of silanol (Si-OH) groups. In general, there is a pH for each metal oxide in aqueous solution where the charges of acidic sites are balanced, known as the point of zero charge ( $\text{pH}_{\text{PZC}}$ ). Above this pH, acidic sites are deprotonated ( $\text{M-O}^-$ , where M=metal); below the  $\text{pH}_{\text{PZC}}$ , protonated ( $\text{M-OH}_2^+$ ) acidic sites dominate the surface. Therefore, the pH of an aqueous solution changes the surface potential of a metal oxide.

The Si 2p spectrum of an aqueous solution of 9 nm diameter  $\text{SiO}_2$  nanoparticles at pH 10 and pH 0.3 are shown in Figure 18. The large component in the spectra is assigned to the bulk Si atoms and neutral Si-OH surface groups. The change in surface potential between these two pH conditions results in a 300 meV shift of this main component. Deprotonation of the silanol groups generates a minority component at lower binding energies in basic conditions (cf. Figure 18a). The protonation of the silanol groups at the acidic pH shifts the minor component to higher binding energies in Figure 18b. The minor component at both pH values is about 13 % of the total intensity. These assignments were aided by density functional theory and are the first direct *in situ* spectroscopic evidence for deprotonated silanol groups. Based on the shift in the main peak and the known relationship between pH and surface potential, [190] 30% of the silanol groups are calculated to be protonated under acidic conditions or deprotonated under basic conditions. This estimation of population is not available from  $^{29}\text{Si}$  NMR data where overlapping peaks prevent species quantification [183].

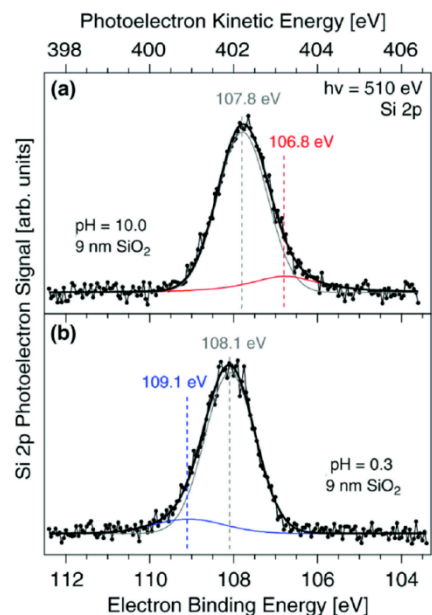


**Figure 18.** Si 2p spectra of liquid jet of an aqueous solution of 10 wt % 9 nm silica nanoparticles at (a) pH 10.0 and (b) pH 0.3. Reprinted with permission from Brown *et al.*, *J. Phys. Chem. C*, 2014, **118**, 29007-16 [183]. Copyright 2014 American Chemical Society.

In the preceding example, the surface potential is modified by a change in the solution pH. For nanoparticles in a liquid jet, it is not possible to directly apply an external potential to the particles. The nanoparticle-in-a-liquid-jet system does, however, have the inherent benefit of fast exchange of the liquid phase, and thus constant pH and solution concentration at the point where photoelectrons are generated in the sample. This will be discussed further in the next example.

#### *Band Alignment at the Solid/Liquid Interface*

Semiconductor/liquid interfaces behave similarly to a semiconductor/metal interface, where a charge separation region in the semiconductor originates from the electronic double layer in the liquid (i.e. band bending). The resulting electric field in the semiconductor influences the core level binding energies. APXPS with tender X-rays has recently been used to probe the energy at the interface between water and an electrode of a photoelectrochemical cell composed of a layer of TiO<sub>2</sub> on boron-doped p-type silicon substrate (p<sup>+</sup>-SiO<sub>2</sub>/TiO<sub>2</sub> electrode) [146]. The substrate and the energy levels of each sample component are illustrated in Figure 19a and 19b, respectively. TiO<sub>2</sub> core level binding energies are dependent on the band bending that results from the liquid double layer, and the liquid binding energies shift with an applied potential, U.

Using the dip-and-pull method shown in Figure 14, a thin layer of aqueous electrolyte was grown on the  $p^+$ -SiO<sub>2</sub>/TiO<sub>2</sub> electrode, and core level spectra were collected while applying a potential ranging from -1.2 V to +0.4 V. The relative binding energy shift of the O 1s peak of the liquid H<sub>2</sub>O (from the 1 M KOH electrolyte) and the O 1s and Ti 2p peaks of the TiO<sub>2</sub> are plotted in Figure 20. As expected from Figure 19b, the water O 1s binding energy shifts with U. The binding energies of the TiO<sub>2</sub> have a more complex behavior that can be divided into four regions, as shown in Figures 20 and 21. Applied potentials in region U<sub>1</sub>, the most negative, result in no shift of the TiO<sub>2</sub> peaks because surface states of the conduction band are filled with electrons and pin the E<sub>F</sub> to the conduction band minimum (cf. Figure 21a). Standard semiconductor behavior occurs at potentials between -1.0 and -0.6 V (region U<sub>2</sub>), where band bending shifts the TiO<sub>2</sub> peaks. Upon Fermi level pinning of the conduction band in Region U<sub>3</sub>, the peak positions again remain constant. In Region U<sub>4</sub> the standard semiconductor behavior returns with shifts in the TiO<sub>2</sub> peaks. Figure 21 illustrates how the energy levels of the water double layer and the applied potential affect the E<sub>F</sub> and conduction band of TiO<sub>2</sub>.

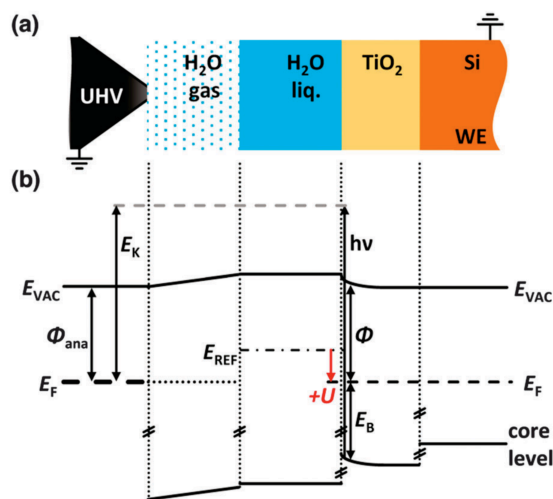


**Figure 19.** (a) Diagram of the SiO<sub>2</sub>/TiO<sub>2</sub> electrode with the aqueous electrolyte layer (1 M KOH) in equilibrium with water vapor. Both the aperture and the electrode are connected to ground. (b) Energy level diagram of the layers of the sample.  $\Phi$  is the work function of the electrode,  $\Phi_{\text{ana}}$  is the work function of the analyzer, and U is the applied potential on the electrode. Reproduced from Lichterman *et al.*, *Energy*

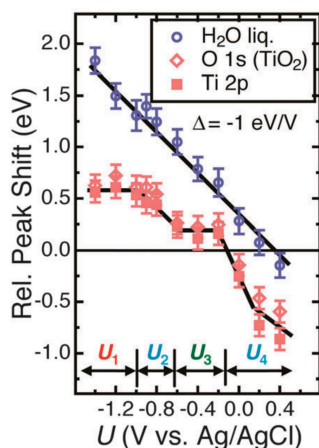


**Figure 20.** Binding energy shifts of the water (blue circles), O 1s of the  $\text{TiO}_2$  (pink diamonds), and the Ti 2p (pink squares) with the applied potential,  $U$ , on the  $\text{p}^+\text{-SiO}_2/\text{TiO}_2$  electrode. Four different potential regions are labelled based on changes in the  $\text{TiO}_2$  binding energy shifts. Reproduced from Lichterman *et al.*, *Energy Environ. Sci.*, 2015, **8**, 2409-16 [146]. Published by the Royal Society of Chemistry. <http://dx.doi.org/10.1039/C5EE01014D>

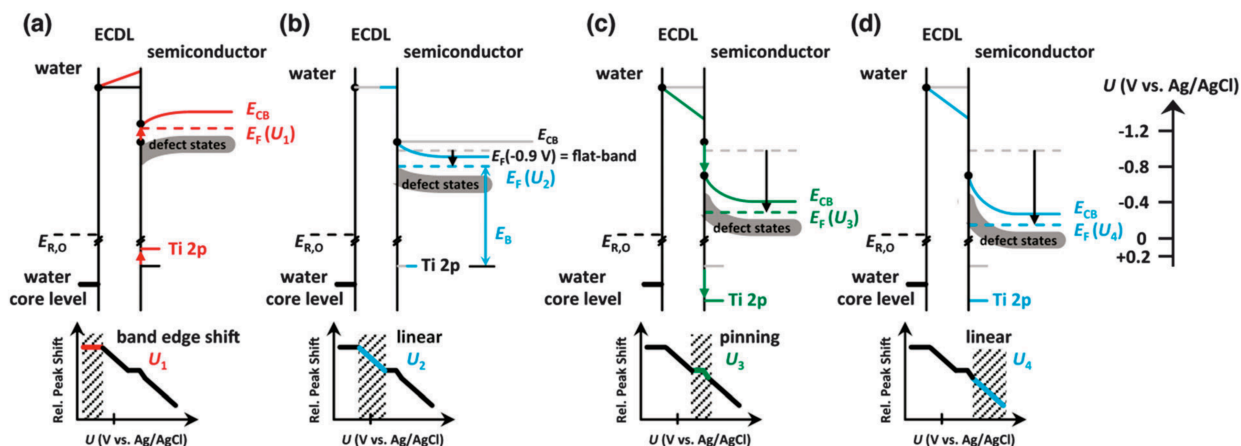


**Figure 21.** Energy level diagrams of the electrode and aqueous layer at the different potential regions identified in Figure 20. (a) Region  $U_1$  (less than -0.9 V) comprises  $\text{TiO}_2$  band bending, (b) Region  $U_2$  (-0.9 V to -0.6 V) contains ideal semiconductor behavior, (c) Region  $U_3$  (-0.6 V to -0.2 V) pins the Fermi level to the defect states, and (d) Region  $U_4$  ( $>$  -0.2 V) resumes ideal semiconductor behavior. Reproduced from Lichterman *et al.*, *Energy Environ. Sci.*, 2015, **8**, 2409-16 [146]. Published by the Royal Society of Chemistry. <http://dx.doi.org/10.1039/C5EE01014D>



The previous study exemplifies the application of APXPS to investigate fundamentals of energy level alignment at liquid/solid interfaces. The dip-and-pull method has also been recently applied to the study of nickel-iron oxyhydroxides that function as water oxidation electrocatalysts [191]. In this case, an important limitation of the dip-and-pull method with regard to certain electrochemical systems becomes apparent – it is possible to measure the chemical nature of these catalysts only at low current densities (i.e. far from some of the technologically relevant conditions). The geometry of the thin electrolyte film in the dip-and-pull method is such that ohmic losses through the liquid film are large and diffusion of ions into and out of the liquid film is slow. The result is a large potential drop and consumption of  $\text{OH}^-$  ions in the liquid layer, the latter of which changes the local pH in the thin electrolyte film. Changes in the electrochemical cell design to decrease ohmic losses and facilitate ion transport, while still allowing for efficient collection of photoelectrons and escape of gas-phase reaction products, is a persistent challenge to investigating these electrocatalysts under technologically relevant conditions.

#### *Sub-nm Depth Resolution with Standing Waving Ambient Pressure XPS*

Regardless of the sample preparation method, photoelectrons from the narrow liquid/solid interface are emitted simultaneously with those from both bulk phases and convoluted with depth-dependent signal attenuation. Depth profiling by changing the photon energy or emission angle only slightly enhances the interface signal, and quantitative information about the interface is difficult to obtain. Sub-nm resolution of chemical species at the liquid/solid interface has been recently obtained by combining standing-wave photoemission spectroscopy [192-194] with APXPS [165,179]. In this technique, a substrate with a buried multilayer mirror (Figure 22) generates a standing wave by interference of the incoming and reflected X-rays. The standing wave propagates perpendicular to the interface and acts as a ruler for the distribution of chemical species. Photoemission spectra are collected as the sample angle is scanned through the first order Bragg angle. The spectral intensity of the chemical species depends on the depth distribution above the multilayer mirror, and plotting this intensity versus angle generates plots known as rocking curves. Simulations of chemical speciation as a function of depth are used to fit the rocking curves and establish the depth distribution of all species below, in, and above the interface. This technique was pioneered examining solid/solid interfaces [192-194].

An example of standing-wave ambient pressure photoemission spectroscopy (SWAPPS) measures the swelling of a Ni surface to a Ni oxyhydroxide in basic conditions under a +0.6 V potential [165]. A layer of Ni (~8 nm) was deposited on the SiO<sub>2</sub> capping layer of the mirror substrate. The Ni 2p<sub>3/2</sub> spectrum of the prepared substrate in UHV (“dry” in Figure 23) shows that the Ni is largely metallic. However, overlapping broad peaks in the O 1s spectrum in Figure 23 indicate the presence of a thin oxide/hydroxide layer. The rocking curves of the metallic Ni 2p<sub>3/2</sub> and oxide O 1s intensity are plotted in Figure 23. Iterative fits of the rocking curves (solid line in Figure 24) reveal that 1.8 nm of the surface is oxidized, depicted in the diagram in Figure 25.

In a water pressure of 17 mTorr (85% relative humidity, “humid” spectra in Figure 23), the Ni is still largely metallic with a thin oxide/hydroxide layer. The water vapor peak prominently appears in the O 1s spectrum at 536 eV (Figure 23), and a contribution from adsorbed liquid water on the surface broadens the oxide/hydroxide signal. The sample was further oxidized by immersion in a 0.1 M KOH solution with cyclic voltammetry cycles between +0.65 and –0.9 V. Using the meniscus method (Figure 14), spectra were collected in the presence of a 20 nm layer of KOH at +0.6 V bias (“immersed” in Figure 23). Characteristic of Ni oxide/hydroxide/oxyhydroxide, the Ni 2p<sub>3/2</sub> binding energy increased to 856 eV. The liquid water signal is more discernable in the O 1s spectrum in Figure 15. Rocking curves of the Ni 3p and liquid O 1s signal are shown in Figure 24 and were used to calculate the thicknesses of the sample components, shown in Figure 25. The 8 nm Ni film expanded to a 27 nm oxide/hydroxide layer. With the standing wave used as an intrinsic ruler, the SWAPPS technique provides sub-nm description of species a solid/liquid interfaces.

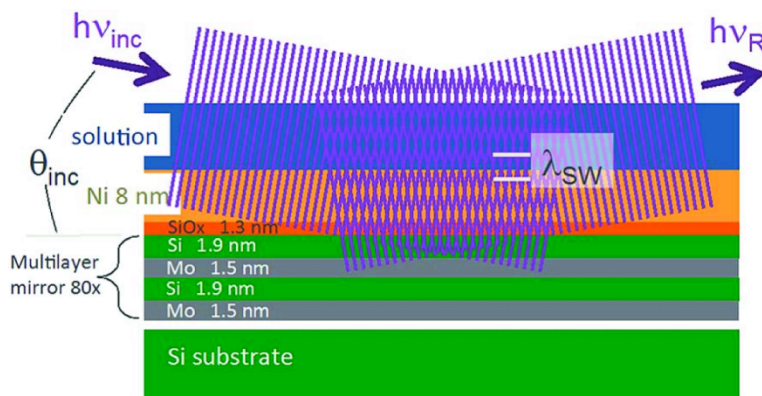


**Figure 22.** Schematic drawing of the multilayer mirror sample and the interaction between the incoming photon beam ( $h\nu_{inc}$ ) and the reflected photon beam ( $h\nu_r$ ) to make a standing wave ( $\lambda_{sw}$ ). The multilayer mirror consists of 80 repetitions of 1.9 nm of Si and 1.5 nm of Mo. A 1.3 nm silicon oxide capping layer separates the mirror from the deposited metal of interest, 8 nm of Ni. Scanning the incident angle ( $\theta_{inc}$ ) through half a period of the standing wave around the Bragg angle ( $\sim 3.4^\circ$ ) results in changes of photoelectron intensity that is plotted in rocking curves and analyzed to yield depth resolution of chemical speciation. Reproduced from [145] with permission from the Royal Society of Chemistry.

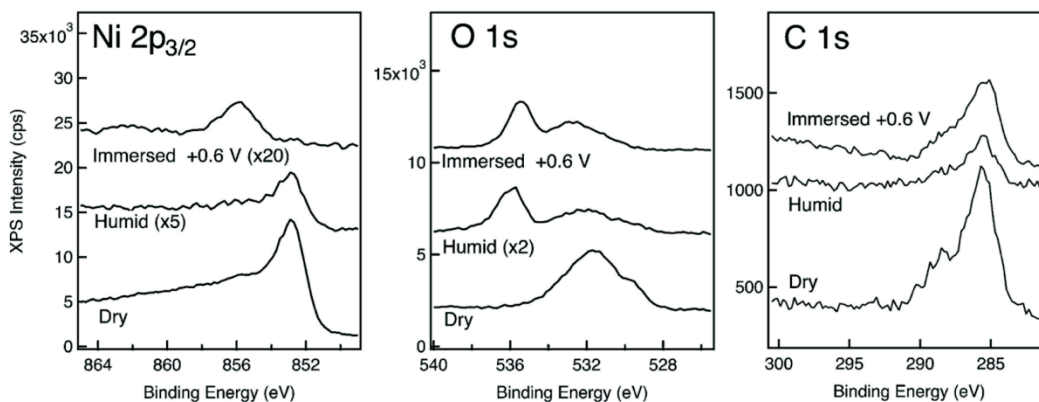


**Figure 23.** Ni 2p<sub>3/2</sub>, O 1s, and C 1s photoemission spectra of the Ni-coated multilayer mirror taken under low vacuum conditions (dry), at a water pressure of 17 Torr (humid), and with a thin KOH film prepared from the meniscus method and an applied potential of +0.6 V<sub>Ag/AgCl</sub> (immersed). The photon energy used was 3100 eV. Reproduced from [145] with permission from the Royal Society of Chemistry.

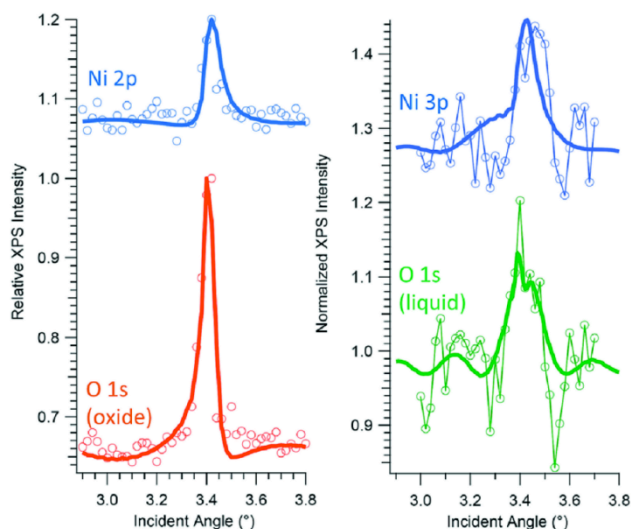


**Figure 24.** Rocking curves (dots) and their simulation (lines) from the photoemission signal (Ni 2p, Ni 3p, O 1s of  $\text{NiO}_x(\text{OH})_y$ , and O 1s of water) from the Ni-coated multilayer mirror (cf. Figure 22) with a thin aqueous KOH film and +0.6  $V_{\text{Ag}/\text{AgCl}}$  applied potential. Reproduced from [145] with permission from the Royal Society of Chemistry.

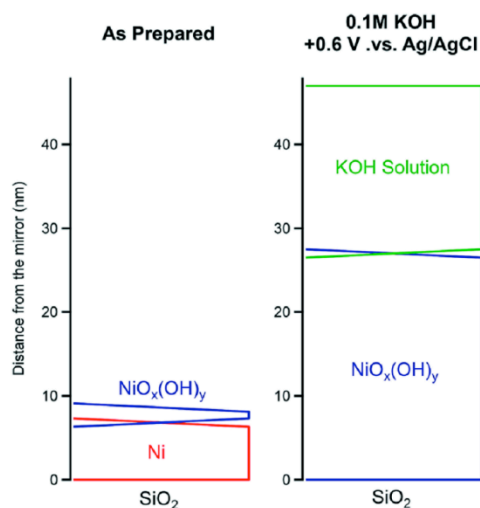


**Figure 25.** Depth profiles of the chemical composition of the Ni-coated multilayer mirror resulting from the rocking curve analysis. The right panel is under low vacuum conditions and the left panel is with a thin film of 0.1 M KOH solution and a +0.6  $V_{\text{Ag}/\text{AgCl}}$  applied potential. Reproduced from [145] with permission from the Royal Society of Chemistry.

Despite the strengths of this technique, SWAPPS suffers from two distinct limitations. First, it is necessary to collect multiple core level spectra at multiple different sample angles. Combining this requirement with the higher energy X-rays required to probe the liquid/solid interface and the signal attenuation by the liquid and vapor phases results in longer acquisition

times for each spectrum and thus very long total experiment times (on the order of several hours per sample condition) when compared to typical APXPS investigations. Maintaining stability of the liquid layer for such a long period of time is challenging, and the effects of beam-induced sample damage must be monitored closely. Secondly, a multi-layer X-ray mirror substrate is required for generation of the standing wave. The sample preparation steps (e.g. deposition, annealing, electrochemical cleaning) must not alter the substrate in such a way as to destroy the standing wave effect, which greatly limits the types of samples that can be studied using this method.

In summary, the discussion in this section shows the obstacles to the measurement of liquid/solid interfaces, mainly given by the necessity to prepare either very thin solid or liquid layers that permit detection of photoelectrons from the interfacial region. In addition, the enhancement of the interfacial signal over that originating from the adjacent bulk phases is a persistent challenge.

## Outlook

As we have discussed in the previous sections, the applications of APXPS are constantly being expanded to new experimental systems and conditions. In particular, advancements in APXPS hardware, new synchrotron capabilities and laboratory X-ray sources with increased brightness have the potential to provide improved time- and spatial-resolution across multiple length scales. Some preliminary examples of this have already been demonstrated. For example, recent measurements demonstrated sub-nanosecond time resolution using the existing APXPS end station hardware available at the ALS beamline 11.0.2 [195,196], While these initial reports only explicitly test the time-resolved capabilities under UHV conditions, experiments in the presence of gases are currently in progress. The development of these capabilities is in particular important for the observation of intermediates in a catalytic reaction, as demonstrated recently under UHV conditions using a 4<sup>th</sup> generation light source [197].

With lab-based APXPS systems which are now commercially available [23,24], access to APXPS as a routine spectroscopic tool is anticipated to increase in the coming years. For any given system, one can make the argument that a lab or synchrotron X-ray source may be preferable, as they both have distinct strengths and drawbacks. For example, one can generally achieve better spatial focusing of the incident X-rays with a synchrotron beamline compared to a monochromatized laboratory (X-ray anode) source. With a synchrotron source, the excitation energy can be selected for non-destructive depth profiling, or can be tuned such that the kinetic energy of the photoelectrons (and thus the probing depth) is constant for each core level measured. On the other hand, the high brightness of synchrotron sources can significantly increase photon-induced damage to biological or other delicate samples. Also, access to synchrotron beamlines in general more limited than access to a lab-based source at one's home institute. Limited synchrotron access is a drawback for high-risk experiments and for long term studies such as mapping complex phase diagrams. Several reports have already been published demonstrating the value and validity of the lab-based APXPS instruments,[198,199] in particular with new operating modes for the electrostatic lens that show promise for a substantial increase of the count rate at a given pressure and kinetic energy [144].

Among the persistent challenges in APXPS is the measurement of insulating samples, such as oxides, due to strong charging, even in the presence of a gas environment. Traditional

UHV systems are commonly equipped with an electron flood gun to facilitate charge dissipation at the sample surface. However, in an APXPS system, the higher pressures preclude use of a standard electron gun that also requires high vacuum conditions (typically  $<10^{-4}$  Torr) to operate. While the ionization of gas molecules via absorption processes will assist with charge dissipation, the resulting spectra can still suffer significantly from binding energy shifts and broadening of photoelectron spectral lines due to charging, in particular inhomogeneous charging, at the sample surface. It is also possible to induce partial charge dissipation by moderate heating of the sample during XPS measurements [200]. However, sample heating is not always an acceptable option due to e.g. thermal instability (decomposition) of certain sample materials or possible reactivity between chemical phases at elevated temperatures. Additionally, heating the sample in many cases takes the APXPS experimental conditions outside of the range of the environmentally or technologically relevant conditions of interest. To circumvent the charging issue, improvements in hardware are under way to develop electron flood guns for operation under higher ambient pressures [23].

Great strides have been made over the past years in increase the pressure limit in APXPS. The goal of measurements at 1 bar can be achieved using two strategies: either by placing an electron-permeable but gas-impermeable membrane between the electron spectrometer and the sample, or by reducing the entrance aperture size of the electrostatic lens system such that the sample can be brought into sufficiently close vicinity to reduce electron scattering to an acceptable level, even at 1 bar. The former strategy has recently been demonstrated [37]. For the latter strategy one can estimate, based on routinely achieved signal-to-noise levels at Torr pressures, that with an aperture size of  $\sim 10$   $\mu\text{m}$  and a sample-to-aperture distance of 20  $\mu\text{m}$  (to assure correct pressure conditions at the sample surface), measurements at atmospheric pressure should be possible. This strategy requires X-ray beams similar in size to the entrance aperture for efficient operation, but these are now routinely available at modern synchrotron sources.

Finally, the development of imaging APXPS will be one of the next frontiers in the field, driven by the necessity to measure the local (instead of the average) chemical and electronic properties of inhomogeneous, technologically/environmentally relevant samples [174] to obtain information on the active sites for surface chemical reactions. Both full-field and scanning microscopy are feasible and are being considered in a number of laboratories. With all these

new developments under way, we are convinced that the reach of APXPS measurements will further expand over the years to come.

### **Acknowledgements**

L.T. and A.R.H. acknowledge funding by the Department of Defense under Grant HDTRA11510005. L.K. acknowledges support from the Danish Research Council for Independent Research and Innovation Fund Denmark (under the National Initiative for Advanced Graphene Coatings and Composites). O.K. and H.B. acknowledge support by the Director, Office of Science, Office of Basic Energy Sciences, and by the Division of Chemical Sciences, Geosciences and Biosciences of the U.S. Department of Energy at LBNL under Contract No. DE-AC02-05CH11231.



## References

- (1) Duke C B (ed.) 1994 *Surface Science: The First Thirty Years* [Special Edition] *Surf. Sci.* **299**.
- (2) Chalk S G, Miller J F and Wagner F W 2000 *J. Power Sources* **86** 40
- (3) Dingerdissen U, Martin A, Herein D, and Wernicke H J 2008 *The Development of Industrial Heterogeneous Catalysis (Handbook of Heterogeneous Catalysis)* (Weinheim: Wiley-VCH)
- (4) Reuter K and Scheffler M 2003 *Phys. Rev. B* **68** 045407
- (5) Ertl G, Knözinger H, Schüth F and Weitkamp J (eds.) 2014 *Handbook of Heterogeneous Catalysis* (Weinheim: Wiley-VCH)
- (6) Kuhlenbeck H, Shaikhutdinov S and Freund H-J 2013 *Chem. Rev.* **113** 3986
- (7) Nilius N, Risse T, Schauer mann S, Shaikhutdinov S, Sterrer M and Freund H-J 2011 *Top. Catal.* **54** 4
- (8) Shen Y R 1989 *Nature* **337** 519
- (9) Rupprechter G 2007 *MRS. Bull.* **32** 1031
- (10) Binnig G, Quate C F and Gerber C 1986 *Phys. Rev. Lett.* **56** 930
- (11) Hu J, Xiao X-D, Ogletree D F and Salmeron M 1995 *Science* **268** 267
- (12) Hendriksen B L M and Frenken J W M 2002 *Phys. Rev. Lett.* **89** 046101
- (13) Hansen T W, Wagner J B, Hansen P L, Dahl S, Topsøe H and Jacobsen C J H 2001 *Science* **294** 1508
- (14) Donald A M 2003 *Nat. Mater.* **2** 511
- (15) Shavorskiy A, Aksoy F, Grass M E, Liu Z, Bluhm H and Held G 2011 *J. Am. Chem. Soc.* **133** 6659
- (16) NIST Electron Inelastic-Mean-Free-Path Database Version 1.2 2010 (Gaithersburg, Md: National Institute of Standards and Technology) (Accessed June 8, 2016)
- (17) Siegbahn H and Siegbahn K 1973 *J. Electron Spectrosc.* **2** 319
- (18) Siegbahn H 1985 *J. Phys. Chem.* **89** 897
- (19) Joyner R W, Roberts M W and Yates K 1979 *Surf. Sci.* **87** 501
- (20) Ruppender H J, Grunze M, Kong C W and Wilmers M 1990 *Surf. Inter. Anal.* **15** 245
- (21) Bluhm H, Hävecker M, Knop-Gericke A, Kleimenov E, Schlögl R, Teschner D, Bukhtiyarov V I, Ogletree D F and Salmeron M 2004 *J. Phys. Chem. B* **108** 14340
- (22) Ogletree D F, Bluhm H, Lebedev G, Fadley C S, Hussain Z and Salmeron M 2002 *Rev. Sci. Instrum.* **73** 3872
- (23) SPECS Surface Nano Analysis GmbH, Berlin, Germany [www.specs.de](http://www.specs.de)
- (24) ScientaOmicron GmbH, Taunusstein, Germany [www.scientaomicron.com/en/products/414/1307](http://www.scientaomicron.com/en/products/414/1307)
- (25) Shavorskiy A, Karshloğlu O, Zegkinoglou I and Bluhm H 2014 *Synchrotron Radiat. News* **27** 14
- (26) Starr D E, Liu Z, Hävecker M, Knop-Gericke A and Bluhm H 2013 *Chem. Soc. Rev.* **42** 5833

- (27) Bluhm H, Hävecker M, Knop-Gericke A, Kiskinova M, Schlögl R and Salmeron M 2007 *MRS. Bull.* **32** 1022
- (28) Salmeron M and Schlögl R 2008 *Surf. Sci. Rep.* **63** 169
- (29) Bluhm H 2010 *J. Electron Spectrosc.* **177** 71
- (30) Knop-Gericke A *et al.* 2009 *Chapter 4 - X-ray Photoelectron Spectroscopy for Investigation of Heterogeneous Catalytic Processes (Advances in Catalysis vol 52)* (Waltham, MA: Academic Press)
- (31) Starr D E, Bluhm H, Liu Z, Knop-Gericke A and Hävecker M 2013 *Application of Ambient Pressure X-Ray Photoelectron Spectroscopy for the in-situ Investigation of Heterogeneous Catalytic Reactions (In-Situ Characterization of Heterogeneous Catalysts)* Rodriguez J A, Hanson J C, Chupas P J (eds.) (New York: John Wiley & Sons)
- (32) Shavorskiy A and Bluhm H 2013 *Ambient Pressure X-Ray Photoelectron Spectroscopy (Handbook of Heterogeneous Catalysts for Clean Technology - Design, Analysis, and Application)* Wilson K, Lee A (eds.) (Weinheim, Germany: Wiley-VCH)
- (33) Head A R and Bluhm H 2016 *Ambient Pressure X-Ray Photoelectron Spectroscopy (Elsevier Reference Module in Chemistry, Molecular Sciences and Chemical Engineering)* Reedijk J (ed.) (Waltham, MA: Elsevier)
- (34) Crumlin E J, Bluhm H and Liu Z 2013 *J. Electron Spectrosc.* **190** 84
- (35) Knudsen J, Andersen J N and Schnadt J 2016 *Surf. Sci.* **646** 160
- (36) Crumlin E J, Liu Z, Bluhm H, Yang W, Guo J and Hussain Z 2015 *J. Electron Spectrosc.* **200** 264
- (37) Weatherup R S, Eren B, Hao Y, Bluhm H and Salmeron M B 2016 *J. Phys. Chem. Lett.* **7** 1622
- (38) Bluhm H, Havecker M, Knop-Gericke A, Kiskinova M, Schlogl R and Salmeron M 2007 *MRS. Bull.* **32** 1022
- (39) Stoerzinger K A, Hong W T, Crumlin E J, Bluhm H and Shao-Horn Y 2015 *Accounts Chem. Res.* **48** 2976
- (40) Ryo T and Hiroshi K 2015 *J. Phys.: Condens. Matter* **27** 083003
- (41) Liu X, Yang W and Liu Z 2014 *Adv. Mater.* **26** 7710
- (42) Velasco-Velez J J *et al.* 2015 *Angew. Chem. Int. Edit.* **54** 14554
- (43) Rocha T C R, Hävecker M, Knop-Gericke A and Schlögl R 2014 *Journal of Catalysis* **312** 12
- (44) Crumlin E J, Mutoro E, Hong W T, Biegalski M D, Christen H M, Liu Z, Bluhm H and Shao-Horn Y 2013 *J. Phys. Chem. C* **117** 16087
- (45) Casalongue H S, Kaya S, Viswanathan V, Miller D J, Friebel D, Hansen H A, Nørskov J K, Nilsson A and Ogasawara H 2013 *Nat. Commun.* **4**
- (46) Casalongue H G S *et al.* 2014 *J. Phys. Chem. C* **118** 29252
- (47) Malacrida P *et al.* 2015 *Phys. Chem. Chem. Phys.* **17** 28121
- (48) Kahk J M *et al.* 2015 *J. Electron Spectrosc.* **205** 57
- (49) Velasco-Vélez J J *et al.* 2016 *Rev. Sci. Instrum.* **87** 053121
- (50) Nilsson A 2002 *J. Electron Spectrosc. Rel. Phenom.* **126** 3
- (51) Blomberg S *et al.* 2013 *Phys. Rev. Lett.* **110** 117601
- (52) Söderström J *et al.* 2012 *Phys. Rev. Lett.* **108** 193005
- (53) Gelius U and Siegbahn K 1972 *Faraday Discuss. Chem. Soc.* **54** 257
- (54) Bischler U and Bertel E 1993 *J. Vac. Sci. Technol. A* **11** 458

- (55) Nikitin A, Ogasawara H, Mann D, Denecke R, Zhang Z, Dai H, Cho K and Nilsson A 2005 *Phys. Rev. Lett.* **95** 225507
- (56) Johansson G, Hedman J, Berndtsson A, Klasson M and Nilsson R 1973 *J. Electron Spectrosc.* **2** 295
- (57) Bird R J and Swift P 1980 *J. Electron Spectrosc.* **21** 227
- (58) Ogletree D F, Bluhm H, Hebenstreit E D and Salmeron M 2009 *Nucl. Instrum. Meth. A* **601** 151
- (59) Starr D E, Wong E K, Worsnop D R, Wilson K R and Bluhm H 2008 *Phys. Chem. Chem. Phys.* **10** 3093
- (60) Yamamoto S *et al.* 2007 *J. Phys. Chem. C* **111** 7848
- (61) Kaya S, Ogasawara H, Näslund L-Å, Forsell J-O, Casalongue H S, Miller D J and Nilsson A 2013 *Catal. Today* **205** 101
- (62) Thomas III J H 1998 *Photon Beam Damage and Charging at Solid Surfaces (Beam Effects, Surface Topography, and Depth Profiling in Surface Analysis vol. 5)* (New York: Plenum Press)
- (63) Yamamoto S, Bluhm H, Andersson K, Ketteler G, Ogasawara H, Salmeron M and Nilsson A 2008 *J. Phys.: Condens. Matter* **20** 184025
- (64) Ketteler G, Yamamoto S, Bluhm H, Andersson K, Starr D E, Ogletree D F, Ogasawara H, Nilsson A and Salmeron M 2007 *J. Phys. Chem. C* **111** 8278
- (65) Todorova M *et al.* 2003 *Surf. Sci.* **541** 101
- (66) Kostelník P, Seriani N, Kresse G, Mikkelsen A, Lundgren E, Blum V, Šikola T, Varga P and Schmid M 2007 *Surf. Sci.* **601** 1574
- (67) Yu Y, Mao B, Geller A, Chang R, Gaskell K, Liu Z and Eichhorn B W 2014 *Phys. Chem. Chem. Phys.* **16** 11633
- (68) Zhang C *et al.* 2010 *Nat. Mater.* **9** 944
- (69) Bozzini B, Amati M, Gregoratti L and Kiskinova M 2013 *Sci. Rep.* **3** 2848
- (70) Bauer E 2012 *J. Electron Spectrosc.* **185** 314
- (71) Novoselov K S, Jiang D, Schedin F, Booth T J, Khotkevich V V, Morozov S V and Geim A K 2005 *P. Natl. Acad. Sci. USA* **102** 10451
- (72) Song L *et al.* 2010 *Nano Lett.* **10** 3209
- (73) Mak K F, Lee C, Hone J, Shan J and Heinz T F 2010 *Phys. Rev. Lett.* **105** 136805
- (74) Wang Q H, Kalantar-Zadeh K, Kis A, Coleman J N and Strano M S 2012 *Nat. Nanotechnol.* **7** 699
- (75) Vogt P, De Padova P, Quaresima C, Avila J, Frantzeskakis E, Asensio M C, Resta A, Ealet B and Le Lay G 2012 *Phys. Rev. Lett.* **108** 155501
- (76) Novoselov K S, Geim A K, Morozov S V, Jiang D, Zhang Y, Dubonos S V, Grigorieva I V and Firsov A A 2004 *Science* **306** 666
- (77) Watanabe K, Taniguchi T and Kanda H 2004 *Nat. Mater.* **3** 404
- (78) Radisavljevic B, Radenovic A, Brivio J, Giacometti V and Kis A 2011 *Nat. Nanotechnol.* **6** 147
- (79) Bonaccorso F, Sun Z, Hasan T and Ferrari A C 2010 *Nat. Photonics* **4** 611
- (80) Kuila T, Bose S, Mishra A K, Khanra P, Kim N H and Lee J H 2012 *Prog. Mater. Sci.* **57** 1061
- (81) Pei S F and Cheng H M 2012 *Carbon* **50** 3210
- (82) Stankovich S, Dikin D A, Piner R D, Kohlhaas K A, Kleinhammes A, Jia Y, Wu Y, Nguyen S T and Ruoff R S 2007 *Carbon* **45** 1558

- (83) Lee Y H *et al.* 2012 *Adv. Mater.* **24** 2320
- (84) Reina A, Jia X T, Ho J, Nezich D, Son H B, Bulovic V, Dresselhaus M S and Kong J 2009 *Nano Lett.* **9** 30
- (85) Li X S, Zhu Y W, Cai W W, Borysiak M, Han B Y, Chen D, Piner R D, Colombo L and Ruoff R S 2009 *Nano Lett.* **9** 4359
- (86) Zhang Y, Zhang L Y and Zhou C W 2013 *Accounts Chem. Res.* **46** 2329
- (87) Loginova E, Bartelt N C, Feibelman P J and McCarty K F 2009 *New J. Phys.* **11** 063046
- (88) Luo Z T, Kim S, Kawamoto N, Rappe A M and Johnson A T C 2011 *ACS Nano* **5** 9154
- (89) Kim H, Mattevi C, Calvo M R, Oberg J C, Artiglia L, Agnoli S, Hirjibehedin C F, Chhowalla M and Saiz E 2012 *ACS Nano* **6** 3614
- (90) Preobrajenski A B, Ng M L, Vinogradov A S and Martensson N 2008 *Phys. Rev. B* **78** 073401
- (91) Park Y S, Park J H, Hwang H N, Laishram T S, Kim K S, Kang M H and Hwang C C 2014 *Phys. Rev. X* **4** 031016
- (92) Larciprete R *et al.* 2012 *ACS Nano* **6** 9551
- (93) Ulstrup S, Andersen M, Bianchi M, Barreto L, Hammer B, Hornekaer L and Hofmann P 2014 *2D Mater.* **1** 025002 (16 pp.)
- (94) Schumacher S *et al.* 2013 *Nano Lett.* **13** 5013
- (95) Topsakal M, Sahin H and Ciraci S 2012 *Phys. Rev. B* **85** 155445
- (96) Wlasny I, Dabrowski P, Rogala M, Kowalczyk P J, Pasternak I, Strupinski W, Baranowski J M and Klusek Z 2013 *Appl. Phys. Lett.* **102** 111601
- (97) Petrovic M *et al.* 2013 *Nat. Commun.* **4** 2772
- (98) Achtyl J L *et al.* 2015 *Nat. Commun.* **6** 6539
- (99) Brugger T, Ma H F, Iannuzzi M, Berner S, Winkler A, Hutter J, Osterwalder J and Greber T 2010 *Angew. Chem. Int. Edit.* **49** 6120
- (100) Ng M L, Shavorskiy A, Rameshan C, Mikkelsen A, Lundgren E, Preobrajenski A and Bluhm H 2015 *ChemPhysChem* **16** 923
- (101) Emmez E, Yang B, Shaikhutdinov S and Freund H-J 2014 *J. Phys. Chem. C* **118** 29034
- (102) Nilsson L, Andersen M, Hammer B, Stensgaard I and Hornekaer L 2013 *J. Phys. Chem. Lett.* **4** 3770
- (103) Liang J, Jiao Y, Jaroniec M and Qiao S Z 2012 *Angew. Chem. Int. Edit.* **51** 11496
- (104) Yang S, Feng X, Wang X and Müllen K 2011 *Angew. Chem. Int. Edit.* **50** 5339
- (105) Choi C H, Chung M W, Kwon H C, Park S H and Woo S I 2013 *Journal of Materials Chemistry A* **1** 3694
- (106) Yang Z, Yao Z, Li G, Fang G, Nie H, Liu Z, Zhou X, Chen X a and Huang S 2012 *ACS Nano* **6** 205
- (107) Sheng Z-H, Gao H-L, Bao W-J, Wang F-B and Xia X-H 2012 *Journal of Materials Chemistry* **22** 390
- (108) Lin Z, Waller G H, Liu Y, Liu M and Wong C-p 2013 *Carbon* **53** 130
- (109) Su Y, Zhang Y, Zhuang X, Li S, Wu D, Zhang F and Feng X 2013 *Carbon* **62** 296
- (110) Wang L, Ambrosi A and Pumera M 2013 *Angew. Chem. Int. Edit.* **52** 13818
- (111) Kyhl L, Balog R, Angot T, Hornekær L and Bisson R 2016 *Phys. Rev. B* **93** 115403

- (112) Bocquet F C, Bisson R, Themlin J M, Layet J M and Angot T 2012 *Phys. Rev. B* **85** 201401
- (113) Vattuone L 2013 *High Resolution Electron Energy Loss Spectroscopy (HREELS): A Sensitive and Versatile Surface Tool (Surface Science Techniques)* Bracco G, Holst B (eds.) (Berlin: Springer)
- (114) Lahiri J, Miller T, Adamska L, Oleynik, II and Batzill M 2011 *Nano Lett.* **11** 518
- (115) Weatherup R S, Bayer B C, Blume R, Baetz C, Kidambi P R, Fouquet M, Wirth C T, Schlögl R and Hofmann S 2012 *ChemPhysChem* **13** 2544
- (116) Patera L L *et al.* 2013 *ACS Nano* **7** 7901
- (117) Weatherup R S *et al.* 2014 *J. Am. Chem. Soc.* **136** 13698
- (118) Weatherup R S, Baetz C, Dlubak B, Bayer B C, Kidambi P R, Blume R, Schloegl R and Hofmann S 2013 *Nano Lett.* **13** 4624
- (119) Weatherup R S, Bayer B C, Blume R, Ducati C, Baetz C, Schlögl R and Hofmann S 2011 *Nano Lett.* **11** 4154
- (120) Bae S *et al.* 2010 *Nat. Nanotechnol.* **5** 574
- (121) Lee Y, Bae S, Jang H, Jang S, Zhu S E, Sim S H, Song Y I, Hong B H and Ahn J H 2010 *Nano Lett.* **10** 490
- (122) Kidambi P R, Bayer B C, Blume R, Wang Z J, Baetz C, Weatherup R S, Willinger M G, Schloegl R and Hofmann S 2013 *Nano Lett.* **13** 4769
- (123) Pirkle A *et al.* 2011 *Appl. Phys. Lett.* **99** 122108
- (124) Kidambi P R, Blume R, Kling J, Wagner J B, Baetz C, Weatherup R S, Schloegl R, Bayer B C and Hofmann S 2014 *Chem. Mater.* **26** 6380
- (125) Yao Y X *et al.* 2014 *P. Natl. Acad. Sci. USA* **111** 17023
- (126) Mu R T, Fu Q, Jin L, Yu L, Fang G Z, Tan D L and Bao X H 2012 *Angew. Chem. Int. Edit.* **51** 4856
- (127) Zhang Y H *et al.* 2015 *Nano Lett.* **15** 3616
- (128) Wei M, Fu Q, Wu H, Dong A and Bao X 2016 *Top. Catal.* **59** 543
- (129) Granas E, Andersen M, Arman M A, Gerber T, Hammer B, Schnadt J, Andersen J N, Michely T and Knudsen J 2013 *J. Phys. Chem. C* **117** 16438
- (130) Wei M M, Fu Q, Yang Y, Wei W, Crumlin E, Bluhm H and Bao X H 2015 *J. Phys. Chem. C* **119** 13590
- (131) Tamtogl A, Bahn E, Zhu J D, Fouquet P, Ellis J and Allison W 2015 *J. Phys. Chem. C* **119** 25983
- (132) Jin L, Fu Q, Dong A Y, Ning Y X, Wang Z J, Bluhm H and Bao X H 2014 *J. Phys. Chem. C* **118** 12391
- (133) Stojanov P, Voloshina E, Dedkov Y, Schmitt S, Haenke T and Thissen A 2014 *Procedia Eng.* **93** 8
- (134) Voloshina E N, Dedkov Y S, Torbrugge S, Thissen A and Fonin M 2012 *Appl. Phys. Lett.* **100** 241606
- (135) Grånäs E, Gerber T, Schröder U A, Schulte K, Andersen J N, Michely T and Knudsen J 2016 *Surf. Sci.* **651** 57
- (136) Diaz J G, Ding Y, Koitz R, Seitsonen A P, Iannuzzi M and Hutter J 2013 *Theor. Chem. Acc.* **132** 1350
- (137) Granas E, Knudsen J, Schroder U A, Gerber T, Busse C, Arman M A, Schulte K, Andersen J N and Michely T 2012 *ACS Nano* **6** 9951
- (138) Blume R *et al.* 2014 *Phys. Chem. Chem. Phys.* **16** 25989

- (139) Dong A Y, Fu Q, Wei M M, Liu Y, Ning Y X, Yang F, Bluhm H and Bao X H 2015 *Surf. Sci.* **634** 37
- (140) Yang Y, Fu Q, Wei M M, Bluhm H and Bao X H 2015 *Nano Res.* **8** 227
- (141) Zhang Y H, Wei M M, Fu Q and Bao X H 2015 *Sci. Bull.* **60** 1572
- (142) Oum K W, Lakin M J, DeHaan D O, Brauers T and Finlayson-Pitts B J 1998 *Science* **279** 74
- (143) Knipping E M, Lakin M J, Foster K L, Jungwirth P, Tobias D J, Gerber R B, Dabdub D and Finlayson-Pitts B J 2000 *Science* **288** 301
- (144) Axnanda S *et al.* 2015 *Sci. Rep.* **5** 9788
- (145) Karslıoğlu O *et al.* 2015 *Faraday Discuss.* **180** 35
- (146) Lichterman M F *et al.* 2015 *Energy Environ. Sci.* **8** 2409
- (147) *Handbook of Chemistry and Physics* (64 ed.) 1983 (Cleveland, OH: The Chemical Rubber Company)
- (148) Faubel M, Steiner B and Toennies J P 1997 *J. Chem. Phys.* **106** 9013
- (149) Brown M A, Seidel R, Thurmer S, Faubel M, Hemminger J C, van Bokhoven J A, Winter B and Sterrer M 2011 *Phys. Chem. Chem. Phys.* **13** 12720
- (150) Brown M A, D'Auria R, Kuo I F W, Krisch M J, Starr D E, Bluhm H, Tobias D J and Hemminger J C 2008 *Phys. Chem. Chem. Phys.* **10** 4778
- (151) Bergersen H, Marinho R R T, Pokapanich W, Lindblad A, Bjorneholm O, Saethre L J and Ohrwall G 2007 *J. Phys.: Condens. Matter* **19**
- (152) Wilson K R, Rude B S, Smith J, Cappa C, Co D T, Schaller R D, Larsson M, Catalano T and Saykally R J 2004 *Rev. Sci. Instrum.* **75** 725
- (153) Gardner J A, Watson L R, Adewuyi Y G, Davidovits P, Zahniser M S, Worsnop D R and Kolb C E 1987 *J. Geophys. Res.: Atmos.* **92** 10887
- (154) Worsnop D R, Zahniser M S, Kolb C E, Gardner J A, Watson L R, Van Doren J M, Jayne J T and Davidovits P 1989 *J. Phys. Chem.* **93** 1159
- (155) Weingarth D, Foelske-Schmitz A, Wokaun A and Kötz R 2011 *Electrochem. Commun.* **13** 619
- (156) Wibowo R, Aldous L, Jacobs R M J, Manan N S A and Compton R G 2011 *Chem. Phys. Lett.* **517** 103
- (157) Krieger U K, Marcolli C and Reid J P 2012 *Chem. Soc. Rev.* **41** 6631
- (158) Davis E J 1997 *Aerosol Sci. Tech.* **26** 212
- (159) Ewing G E 2006 *Chem. Rev.* **106** 1511
- (160) Krisch M J, D'Auria R, Brown M A, Tobias D J, Hemminger J C, Ammann M, Starr D E and Bluhm H 2007 *J. Phys. Chem. C* **111** 13497
- (161) Arima K, Jiang P, Deng X, Bluhm H and Salmeron M 2010 *J. Phys. Chem. C* **114** 14900
- (162) Krepelova A, Huthwelker T, Bluhm H and Ammann M 2010 *ChemPhysChem* **11** 3859
- (163) Tissot H, Gallet J-J, Bournel F, Olivieri G, Silly M G, Sirotti F, Boucly A and Rochet F 2015 *Top. Catal.* **59** 605
- (164) Tissot H, Olivieri G, Gallet J J, Bournel F, Silly M G, Sirotti F and Rochet F 2015 *J. Phys. Chem. C* **119** 9253
- (165) Karslıoğlu O *et al.* 2015 *Faraday Discuss.* **180** 35
- (166) Siegbahn H 1985 *J. Phys. Chem.* **89** 897
- (167) Siegbahn H, Svensson S and Lundholm M 1981 *J. Electron Spectrosc.* **24** 205

- (168) Fellnerfeldegg H, Siegbahn H, Asplund L, Kelfve P and Siegbahn K 1975 *J. Electron Spectrosc.* **7** 421
- (169) Moberg R, Boekman F, Bohman O and Siegbahn H O G 1991 *J. Am. Chem. Soc.* **113** 3663
- (170) Bluhm H, Ogletree D F, Fadley C S, Hussain Z and Salmeron N 2002 *J. Phys.: Condens. Matter* **14** L227
- (171) Hüfner S *Photoelectron Spectroscopy: Principles and Applications*; Springer-Verlag Berlin Heidelberg New York, 2003
- (172) Siegbahn H, Lundholm M, Arbman M and Holmberg S 1983 *Phys. Scripta* **27** 241
- (173) Ghosal S, Hemminger J C, Bluhm H, Mun B S, Hebenstreit E L D, Ketteler G, Ogletree D F, Requejo F G and Salmeron M 2005 *Science* **307** 563
- (174) Jungwirth P and Tobias D J 2002 *J. Phys. Chem. B* **106** 6361
- (175) Vrbka L, Mucha M, Minofar B, Jungwirth P, Brown E C and Tobias D J 2004 *Curr. Opin. Colloid In.* **9** 67
- (176) Lee M T, Brown M A, Kato S, Kleibert A, Turler A and Ammann M 2015 *J. Phys. Chem. A* **119** 4600
- (177) Liu Z and Bluhm H 2016 *Liquid/Solid Interfaces Studied by Ambient Pressure HAXPES (Hard X-ray Photoelectron Spectroscopy (HAXPES))* Woicik C J (ed.) (Cham, Switzerland: Springer International Publishing) p 447-466
- (178) Zaera F 2011 *Surf. Sci.* **605** 1141
- (179) Nemšák S *et al.* 2014 *Nat. Commun.* **5**
- (180) Söderström J, Ottosson N, Pokapanich W, Öhrwall G and Björneholm O 2011 *J. Electron Spectrosc.* **184** 375
- (181) Brown M A, Jordan I, Beloqui Redondo A, Kleibert A, Wörner H J and van Bokhoven J A 2013 *Surf. Sci.* **610** 1
- (182) Brown M A, Beloqui Redondo A, Sterrer M, Winter B, Pacchioni G, Abbas Z and van Bokhoven J A 2013 *Nano Lett.* **13** 5403
- (183) Brown M A, Arrigoni M, Héroguel F, Beloqui Redondo A, Giordano L, van Bokhoven J A and Pacchioni G 2014 *J. Phys. Chem. C* **118** 29007
- (184) Olivieri G, Goel A, Kleibert A and Brown M A 2015 *J. Synchrotron Radiat.* **22** 1528
- (185) Kraus J, Reichelt R, Gunther S, Gregoratti L, Amati M, Kiskinova M, Yulaev A, Vlassioug I and Kolmakov A 2014 *Nanoscale* **6** 14394
- (186) Masuda T, Yoshikawa H, Noguchi H, Kawasaki T, Kobata M, Kobayashi K and Uosaki K 2013 *Appl. Phys. Lett.* **103** 111605
- (187) Takagi Y *et al.* 2014 *Appl. Phys. Lett.* **105** 131602
- (188) Wu C H, Weatherup R S and Salmeron M B 2015 *Phys. Chem. Chem. Phys.* **17** 30229
- (189) Kolmakov A, Dikin D A, Cote L J, Huang J, Abyaneh M K, Amati M, Gregoratti L, Gunther S and Kiskinova M 2011 *Nat. Nano.* **6** 651
- (190) Brown M A *et al.* 2013 *Langmuir* **29** 5023
- (191) Ali-Löytty H *et al.* 2016 *J. Phys. Chem. C* **120** 2247
- (192) Fadley C S 2013 *J. Electron Spectrosc.* **190** 165
- (193) Gray A X 2014 *J. Electron Spectrosc.* **195** 399

- (194) Yang S-H, Gray A X, Kaiser A M, Mun B S, Sell B C, Kortright J B and Fadley C S 2013 *J. Appl. Phys.* **113** 073513
- (195) Shavorskiy A *et al.* 2014 *Rev. Sci. Instrum.* **85** 093102
- (196) Neppel S *et al.* 2015 *Ultrafast Phenomena XIX, Springer Proceedings in Physics* **162** 325
- (197) Öström H *et al.* 2015 *Science* **347** 978
- (198) Eriksson S K *et al.* 2014 *Rev. Sci. Instrum.* **85** 075119
- (199) Jürgensen A, Esser N and Hergenröder R 2012 *Surf. Inter. Anal.* **44** 1100
- (200) Price R, Erlep-Erden T, Crumlin E, Rani S, Garcia S, Smith R, Deacon L, Euaruksakul C and Held G 2016 *Top. Catal.* **59** 516